4

Removal of VOCs Using Nonthermal Plasma Technology

Tao Zhu
School of Chemical and Environmental Engineering, China University of Mining& Technology, Beijing 100083, China

1. Introduction

Volatile organic compounds (VOCs) are liquids or solids that contain organic carbon (carbon bonded to carbon, hydrogen, nitrogen, or sulfur, but not carbonate carbon as in $CaCO_3$ nor carbide carbon as in CaC_2 or CO_2), which vaporize at significant rates. VOCs are probably the second-most widespread and diverse class of emissions after particulates.

VOCs are a large family of compounds. Some (e.g., benzene) are toxic and carcinogenic, and are regulated individually as hazardous pollutants. The control of VOCs in the atmosphere is a major environmental problem now. Toluene and benzene are two of the typical VOCs. They effluents in some industries, such as paints, paint thinners, fingernail polish, lacquers, adhesives, rubber, and some printing and leather tanning processes, have attracted more and more attention of researchers. The traditional methods of VOCs removal such as absorption, adsorption, and incineration and so on, which are referred to the new environmental condition have many technical and economic disadvantages. In these years, some new technologies, such as biologic process, photo-catalysis process, and plasma technology, were paid more and more attention.

As an emerging technology for environmental protection, there have been extensive researches on using non-thermal plasma (NTP) over the past 20 years. The major advantages of NTP technology include the moderate operation conditions (normal temperature and atmospheric pressure), moderate capital cost, compact system, easy operations and short residence times, Etc., compare to the conventional technologies). In the field of air pollution control, the NTP technology has been tested for the abatement of various types of hazardous air pollutants such as volatile organic compounds (VOCs), SO_2, NOx, CFCs, odors, mercury, etc.

In this chapter, we will introduce a new synergy technology basing on non-thermal plasma for VOCs decomposition.

2. Experimental setup

The reaction system was a tube-wire packed-bed reaction system at ambient temperature and atmospheric pressure. The schematic diagram of the NTP system is shown in Fig.1. Dry air (78.5% N_2, 21.5% O_2) was used as a balance gas for VOCs decomposition. Air supplied from an air compressor was divided into two airflows and each flow rate was controlled

with a mass flow meter. One airflow was introduced into a VOCs liquid bottle (3), which contained liquid VOCs. The air with a mass of saturated VOCs vapor was mixed with the other airflow in a blender (4) and the gaseous phase VOCs was diluted to a prescribed concentration. A wire-tube DBD reactor with packed materials as shown in Fig.2 was used.

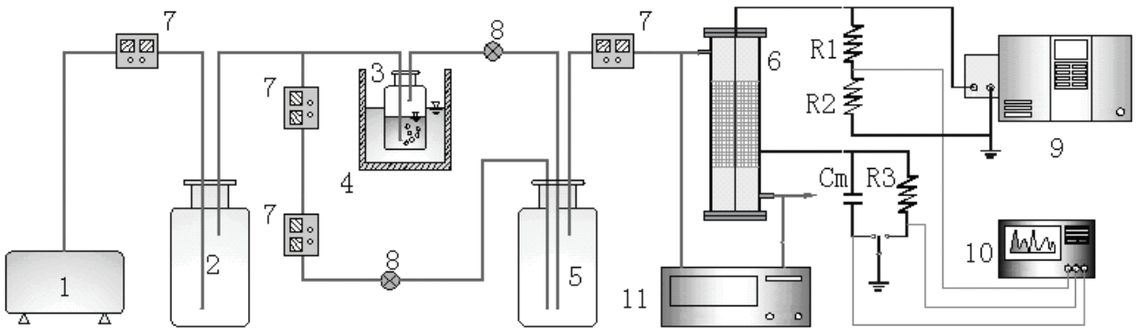

1.air compressor 2.buffer 3.toluene liquid bottle 4.attemperator 5.blender 6.NTP reactor 7.mass flow meter 8.needle valve 9.high voltage 10.oscukkograph 11.gas chromatograph

Fig. 1. Schematic diagram of the NTP system

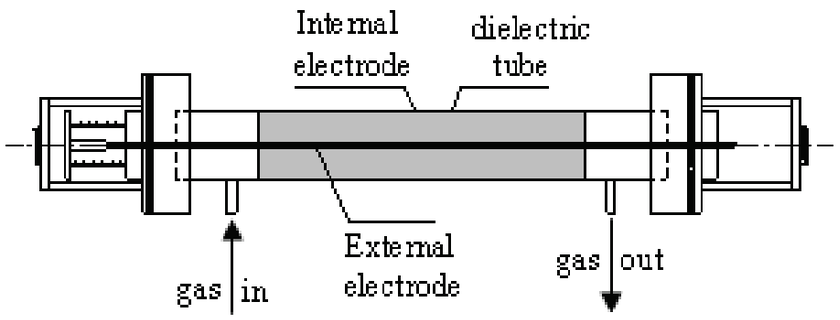

Reactor: organic-glass tube (i.d.50mm, length 150mm)
Internal electrode: tungsten filament (i.d.0.5mm)
External electrode: dense steel mesh

Fig. 2. The NTP reactor

An AC power supply of 150 Hz was employed in the NTP reactor. The AC voltage was applied to the reactor in the radial direction and the voltage extension changed from 0 kV to 50 kV. The voltage and current of the discharge process were detected by an oscillograph (manufactured by American Tektronix Co., TDS2014). Primary power values were measured with the voltage-charge (V-Q)Lissajous method in the plasma reactors. The circuit diagram on power measurement with Lissajous developed and used in this study is shown in figure 3.

To investigate the electric characteristics of dielectric barrier discharge (DBD), the voltage applied to the reactor was sampled by a voltage divider with a ratio of 12500:1. Also, the current was determined from the voltage drop across a shunt resistor (R3 =10kΩ) connected in series with the grounded electrode. In order to obtained the total charge and discharge power simultaneously, a capacitor (Cm =2μF) was inserted between the reactor and the ground. The electrical power provided to the discharge was measured using the Q–V

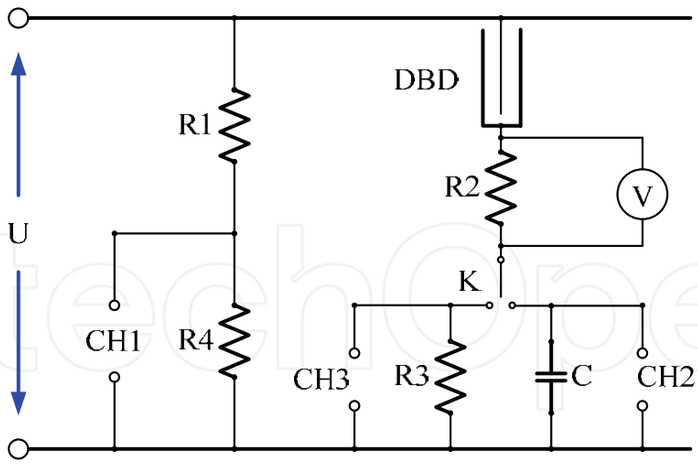

*R*1=250MΩ, *R*2=10KΩ, *R*3=10KΩ, *R*4=20KΩ, *C*=0.33μF,
K—Switch, CH1—Voltage sampling of oscillograph,
CH2—Lissajous sampling of oscillograph,
CH3—Current sampling of oscillograph

Fig. 3. Circuit diagram on power measurement with Lissajous

Lissajous diagram. Typical Lissajous diagram represents to be a parallelogram, and we could calculate power though calculated the area of parallelogram.

VOCs analysis was carried out by gas chromatography (manufactured by Aglient Co., HP6890N) with a flame ionization detector (FID). The byproducts were detected by GC-MS (manufactured by American Thermo Finnegan Co.) using EI mode, 70 eV and full scan. Ozone concentration produced in the NTP reactor was measured by an iodine-titration method. The plasma reactor employed an AC power supply of 50-500Hz scanning from 0 kV to 100 kV was applied to the reactor in the radial direction.

As evaluation criteria, the VOCs removal efficiency, reactor energy density, energy efficiency, the selectivity of CO_2 and the selectivity of CO (eg., benzene) in the gas phase were calculated as follows:

VOCs removal efficiency (η):

$$\eta(\%) = \frac{[VOCs]_{inlet} - [VOCs]_{outlet}}{[VOCs]_{inlet}} \times 100\% \tag{1}$$

Reactor energy density (RED):

$$RED(kJ/L) = \frac{input \cdot power(W)}{gas \cdot flow \cdot rate(L/\min)} \times 60 \times 10^{-3} \tag{2}$$

Energy efficiency (ς):

$$\varsigma(g/kWh) = \frac{[VOCs]_{inlet} \times \eta}{RED} \times 3.6 \times 10^{-3} \tag{3}$$

Selectivity of CO_2 (ζ):

$$\zeta(\%) = \frac{[CO_2]}{6([Benzene]_{inlet} - [Benzene]_{outlet})} \times 100\% \tag{4}$$

Selectivity of CO (ξ):

$$\xi(\%) = \frac{[CO]}{6([Benzene]_{inlet} - [Benzene]_{outlet})} \times 100\% \quad (5)$$

2.1 Adsorption-enhanced Non-thermal Plasma

We previously reported the oxidative decomposition of formaldehyde, benzene, VOCs and odorin air using a plasma reactor packed with various materials. The frequency of the applied high voltage alternating current (AC) had an important influence on energy efficiency and intermediate frequency of the applied AC power was beneficial for VOCs removal, especially 150 Hz.

Urashitnal et al. used NTP packed with active carbon to decompose VOCs and trichoroethylene (TCE) with the discharge energy efficiencies of 26 g/(kW·h) and 13 g/(kW·h), respectively. The TCE removal efficiency was 40% using NTP technology alone and it was up to 90% using NTP packed with active carbon. Ogata et al. found MS-4A molecular griddle played a special role in VOCs removal using NTP technology and reported that the VOCs removal efficiency in the dielectric barrier discharge (DBD) reactor packed with MS-4A molecular griddle and $BaTiO_3$ particles was 1.4~2.1 times higher than that in DBD reactor packed with $BaTiO_3$ particles.

In this experiment, the mechanism of adsorption-enhanced NTP for volatile organic compounds (Toluene) removal was discussed. A sorbent was packed into the space of discharge plasma so that reaction time was prolonged between VOCs molecules and NTP and removal efficiency of VOCs was improved without increasing the size of NTP reactor. The sorbent was helpful for enhancing discharge energy efficiency due to VOCs molecules enrichment on the surface of the sorbent.

2.2 Adsorption kinetics

The pellets of γ-Al_2O_3, 5~7mm in diameters, was used as the sorbent to be packed into the NTP reactor. Figure 4 shows the VOCs concentration profile as a function of time on γ-Al_2O_3 pellets in the NTP reactor before plasma was applied (VOCs: 800 mg/m^3; flow rate: 2 mL/min; dry air). VOCs was adsorbed on the surface of γ-Al_2O_3 and its concentration was gradually increased with time. After 150 min, the VOCs concentration reached the adsorption-desorption equilibrium. So the decomposition tests were initiated after the adsorption-desorption equilibrium.

The collision frequency between adsorption rate (Ra) and adsorbate molecules on the adsorbent surface is proportional to fraction of the vacant active sites on the adsorbent surface (1-θ):

$$R_a = k_{a0} T^{-1/2} (1-\theta) y^0 \quad (6)$$

where $k_{a0} = a/(R/2\pi M)^{1/2}$.

The desorption rate (Rd) is proportional to the fraction of the occupied active sites (θ):

$$R_d = k_{a0} \theta exp(-E_d/RT) \quad (7)$$

And the net-desorption rate of adsorbate molecules should be the difference between the desorption rate and the adsorption rate:

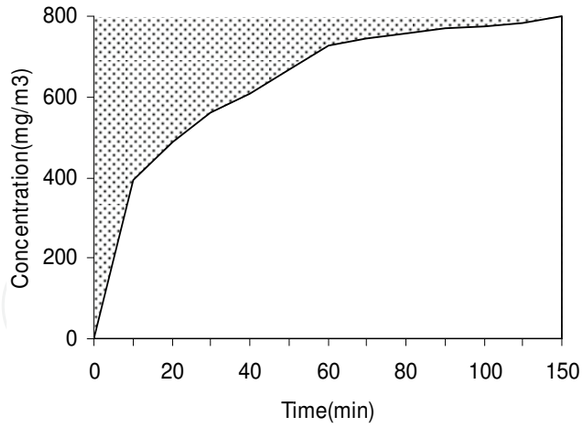

Fig. 4. VOCs concentration on the surface of γ-Al_2O_3 pellets

$$-d\theta/dt=R_d-R_a=k_d\theta-k_a(1-\theta)y^0 \tag{8}$$

where $k_a=k_{a0}T^{-0.5}$ and $k_d=k_{d0}exp(-E_d/RT)$

According to the reaction status on the surface of catalyst in the NTP reactor, adsorbate molecules are in the slow diffusion in the adsorbent channels and the balance between adsorbent surface molecules and gas phase would be established for a long time. In this case, the net adsorption rate can be expressed as:

$$-d\theta/dt=k(y^0-y) \tag{9}$$

During a certain period of time dt, the adsorption process mass balance between the gas and solid phase adsorbent is:

$$F_y M=m_s q_m(-d\theta/dt) \tag{10}$$

The adsorbate molecules in the pores of adsorbent diffuse slowly and the mass transfer rate constant k is smaller. As we known, the desorption temperature is a linear function of the frequency of high voltage and the reaction time:

$$T=T_0+a_H f+\beta_H t \tag{11}$$

By combining Eq.(9), (10) and (11), the coverage rate of adsorbate on the surface of adsorbent as a function of temperature can be obtained:

$$d\theta/dt=(k_d\theta/a_H\beta_H)/\{[-k_a(1-\theta)/k]+[k_a(1-\theta)b-1]\} \tag{12}$$

Where $b=-m_s q_m/FM$.

As mentioned earlier, assuming that the mass transfer coefficient is small enough, the contaminants adsorbed on the surface would be desorped and degraded immediately on the surface of catalyst, that is, $k_a(1-\theta)/k >> [k_a(1-\theta)b-1]$. Then eq.(12) becomes:

$$d\theta/dt=-k\,k_d\,\theta/[a_H\beta_H\,k_a(1-\theta)] \tag{13}$$

When the desorption rate is maximum and $-d^2\theta/dT^2=0$, eq.(13) can be obtained:

$$-d\theta/dT|_{T=Ti}=\theta_i(1-\theta_i)(1/2T_i+E_d/RT_i^2) \tag{14}$$

In the situation of γ-Al_2O_3 adsorption interaction with the plasma, the VOCs concentration in the surface of γ-Al_2O_3 reached adsorption equilibrium. The removal amount of VOCs equaled to 25% of the inlet total concentration of VOCs by adsorption ofγ-Al_2O_3.

2.3 Effect of packed materials on removal efficiency

Figure 5 shows the relationship between reactor energy density (RED) and VOCs removal efficiency with different packed materials in the NTP reactor. The VOCs removal efficiency increased with RED and was in an order of no padding < common packed materials < γ-Al_2O_3. On one hand, γ-Al_2O_3, as a sorbent, could adsorb short-living free redicals. In gas discharge process, these free redicals would accelerate decomposition reactions on the surface of microhole structure of the sorbent. The surface of the cellularity particles could also become active sites with electrons stricking. On the other hand, due to their higher permittivity of 11, γ-Al_2O_3 pellets gained more electric charges and enhanced the local discharge and the discharge current. As a result, γ-Al_2O_3 pellets were helpful for the VOCs removal reaction.

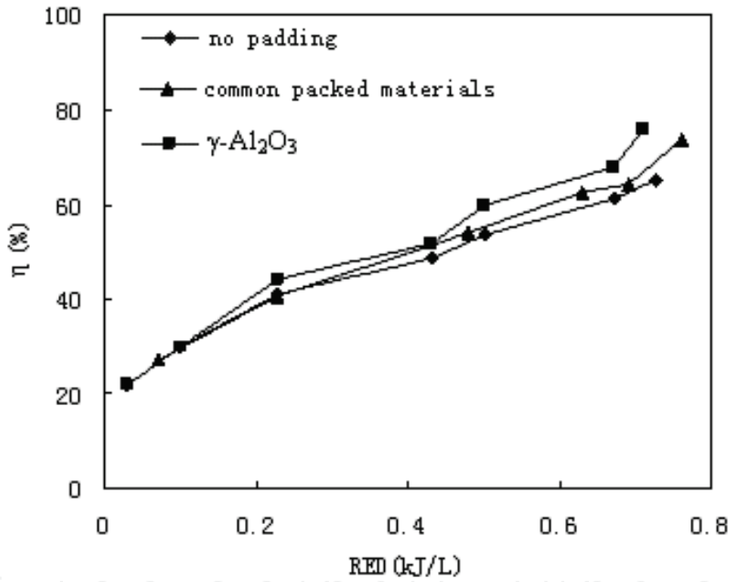

Fig. 5. Relationship between RED and removal efficiency of VOCs with different packed materials

2.4 Effect of packed materials on ozone concentration

Figure 6 shows the relationship between the packed materials and ozone concentration. The effect on the ozone concentration was in an order of γ-Al_2O_3 < no padding < common packed materials at various REDs. The ozone concentration reached the peak at RED of 0.7 kJ/L with the same packed materials in the NTP reactor as shown in figure 6.

High energy electrons produced by gas discharge ionized the VOCs molecules which were adsorbed on the γ-Al_2O_3 surface to produce more positive ions including N^+, N_2^+, O_2^+ and H_3O^+. These positive ions activated VOCs molecules for VOCs decomposition though electric discharge transferring reactions. In the NTP reactor, the VOCs molecules were decomposed by the radicals of $O^\bullet$, $OH^\bullet$ and $N^\bullet$, etc. Evans et al. believed that $O^\bullet$ played a

key role for VOCs decomposition in the NTP process. Ozone as the main long-living radical was transported to the surface of γ-Al_2O_3 and could take part in oxidation reaction. The pathways of reaction were stated as follows:

$$e + O_2 \rightarrow 2O + e \tag{15}$$

$$O + O_2 + M \rightarrow O_3 + M \tag{16}$$

$$O + O_3 \rightarrow 2O_2 \tag{17}$$

$$e + O_3 \rightarrow O + O_2 + e \tag{18}$$

The active oxygen species formed during the O_3 decomposition would also be helpful for the VOCs removal.

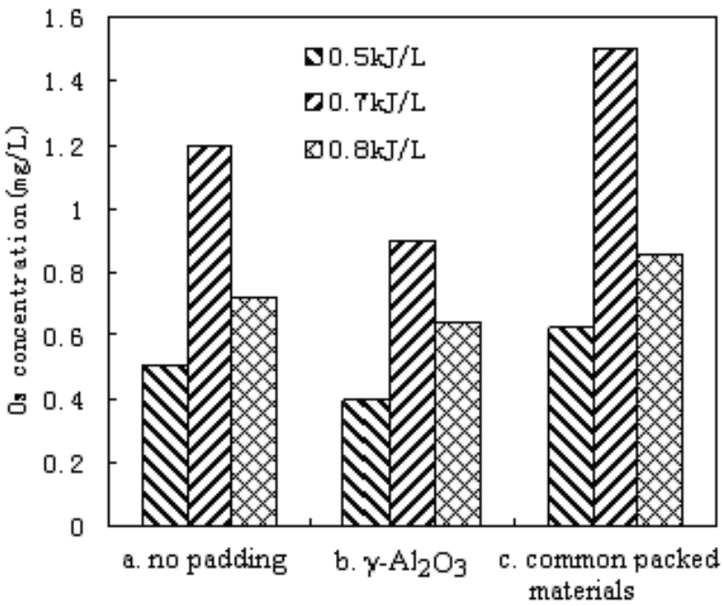

Fig. 6. Relationship between the packed materials and ozone concentration

2.5 Effect of packed materials on energy efficiency

Figure 7 shows the relationship between RED and electric energy efficiency with different packed materials in the NTP reactor. The energy efficiency for VOCs removal decreased with increasing RED and was in an order of no padding < common packed materials < γ-Al_2O_3. Ions, electrons, excited neutral molecules and metastable free radicals in the plasma process attacked the surface of γ-Al_2O_3 pellets and made many kinds of reciprocity possible:

1. The plasma brought sub-electrons launching.
2. The plasma induced chemical reactions on the surface of the γ-Al_2O_3 pellets and produced active atoms, molecules and free radicals, which would take part in chemical reactions for the further VOCs decomposition.
3. Many active oxidation groups in plasma were adsorbed on the surface of the γ-Al_2O_3 pellets. The plasma induced the desorption of VOCs molecules and active oxidation

groups so that further reactions took place. As a result, the whole reaction process was accelerated and more reaction routes were induced.

4. VOCs removal efficiency and electric energy efficiency were improved.

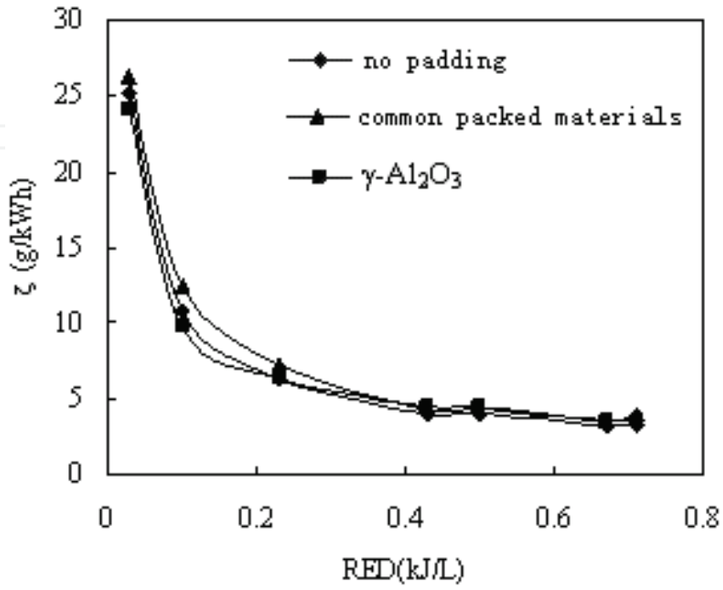

Fig. 7. Relationship between RED and electric energy efficiency with different packed materials

3. Effect of modified ferroelectric on nonthermal plasma process

The major bottleneck of developing NTP with catalysis technology is the reduction of energy consumption. If this requirement is not satisfied, the non-thermal plasma process may lose its potential for commercial applications. In order to resolve this problem, Ayrault et al. used platinum (Pt)-based catalyst supported on an alumina wash-coated honeycomb monolith by means of a high voltage bi-polar pulsed excitation. The energy efficiency was 0.14 mol/kWh at an energy density of 200 J/L for 2-Heptanone decomposition. For a comparison, the energy efficiency decreased to 0.029 mol/kWh using an uncoated monolith even at a higher energy density of 500 J/L.

In this investigation, we developed a new ferroelectric packed bed NTP reactor and prepared a sample of $Ba_{0.8}Sr_{0.2}Zr_{0.1}Ti_{0.9}O_3$ to serve as modified ferroelectrics. The permittivity of $Ba_{0.8}Sr_{0.2}Zr_{0.1}Ti_{0.9}O_3$ was 10^4, 12 times higher than that of the pure phase of $BaTiO_3$, while dielectric loss was 1/6 in room temperature. The experimental results show that this type of modified ferroelectrics packed into the NTP reactor could both reduce the energy consumption and raise energy efficiency significantly. Compared with $BaTiO_3$, $Ba_{0.8}Sr_{0.2}Zr_{0.1}Ti_{0.9}O_3$ had better ferroelectric physical properties to improve NTP process for VOCs control.

3.1 Materials and methods

In the experiment, three kinds of packed materials, including ceramic rings, $BaTiO_3$ rings and $Ba_{0.8}Sr_{0.2}Zr_{0.1}Ti_{0.9}O_3$ rings (hollow cylinder shape, 5 mm i.d., 1 mm wall thick, and 10 mm length), were used to pack into the NTP reactor.

Nano-size $Ba_{0.8}Sr_{0.2}Zr_{0.1}$ $Ti_{0.9}O_3$ powder was prepared using the method of water-thermal composite action at atmospheric pressure. Inorganic salts, including $TiCl_4$, $Ba(OH)_2 \cdot 8H_2O$ and $Sr(OH)_2 \cdot 8H_2O$, were the precursors for $Ba_{0.8}Sr_{0.2}Zr_{0.1}$ $Ti_{0.9}O_3$ formation. Firstly, a proper quantity of $TiCl_4$ was added to 100mL water as the precursor solution and a ammonia used to adjust pH to 7. By strictly controlling the reaction conditions in a ventilation cabinet, the precursor solution hydrolyzed to α-H_2TiO_3. And then, Cl^- was removed by hot water washing and filtrated by decompression and boiled at 100 ^oC for 4 hours. Certain amounts of $Ba(OH)_2 \cdot 8H_2O$ and $Sr(OH)_2 \cdot 8H_2O$ dropped into H_2TiO_3 and ammonia adjusted pH to 6~6.5 and the solution was shielded from air and agitated for hours. During the preparation, if needed, water was added to keep the balance of the liquid quantity. Whereafter, gained solid (nano-$Ba_{0.8}Sr_{0.2}Zr_{0.1}Ti_{0.9}O_3$) was ground to powders and dried at 100 ^oC in a crucible. The powder was made into rings (5 mm i.d., 1 mm wall thick, and 10 mm length) which were placed in a muffle furnace to calcine at 1200 ^oC for two hours. The calcined product was cooled to ambient temperature and served as the packed materials in the NTP reactor. At the same time, a $BaTiO_3$ (powders made in Beijing Research Institute of Chemical Engineering & Metallurgy) ring was also made with the same weight as the $Ba_{0.8}Sr_{0.2}Zr_{0.1}Ti_{0.9}O_3$ ring.
The crystal structure and the surface shape of the $Ba_{0.8}Sr_{0.2}Zr_{0.1}Ti_{0.9}O_3$ sample were detected by XRD (manufactured by Germany Bruker Co., D8 ADVANCE) and SEM (manufactured by Japan, JEOL-JSM-6500F) and the BET surface area determined by Micromeritics (manufactured by American Quantachrome Co., NOVA 1000). The relative permittivity of the $Ba_{0.8}Sr_{0.2}Zr_{0.1}Ti_{0.9}O_3$ sample was measured using an LCR automatism test instrument (manufactured by China, 4210).

3.2 Characteristic of modified ferroelectric

The crystal structure of $Ba_{0.8}Sr_{0.2}Zr_{0.1}Ti_{0.9}O_3$ detected by XRD as shown in Figure 8 should be similar to cube crystal structure of calcium-titanium oxide. $Ba_{0.8}Sr_{0.2}Zr_{0.1}Ti_{0.9}O_3$ was a type of ferroelectric like $BaTiO_3$. The average diameter of sample particulates was of 59 nm. Fig.9 shows that crystal shape of $Ba_{0.8}Sr_{0.2}Zr_{0.1}Ti_{0.9}O_3$ was spherical. The BET surface area of the

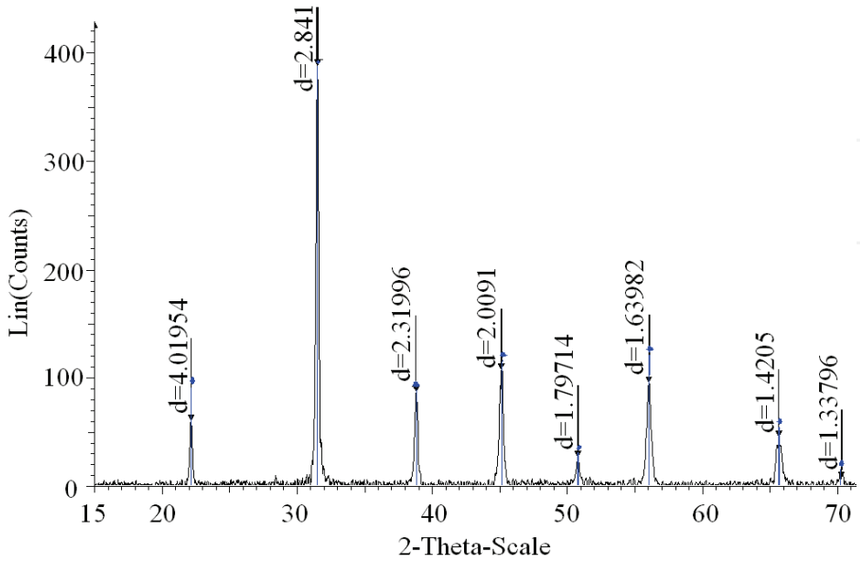

Fig. 8. XRD testing results of $Ba_{0.8}Sr_{0.2}Zr_{0.1}Ti_{0.9}O_3$

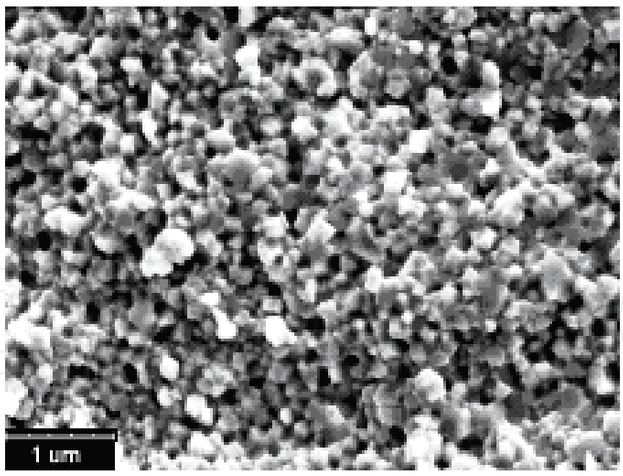

Fig. 9. SEM testing results of $Ba_{0.8}Sr_{0.2}Zr_{0.1}Ti_{0.9}O_3$

$Ba_{0.8}Sr_{0.2}Zr_{0.1}Ti_{0.9}O_3$ powders are 8.8 m^2/g, and Longmuir surface area detected by Micromeritics are 12.3 m^2/g respectively. The relative permittivity of $Ba_{0.8}Sr_{0.2}$ $Zr_{0.1}Ti_{0.9}O_3$ detected by LCR is about 12000.

3.3 Effect of $Ba_{0.8}Sr_{0.2}Zr_{0.1}Ti_{0.9}O_3$ on removal efficiency of toluene

Fig.10 shows the effect of different packed materials in the NTP reactor on the removal efficiency (η) of toluene. The removal efficiency of toluene increases with reactor energy density (RED) and is in the order of without packed materials < with $BaTiO_3$ < with $Ba_{0.8}Sr_{0.2}Zr_{0.1}Ti_{0.9}O_3$, at the same RED.

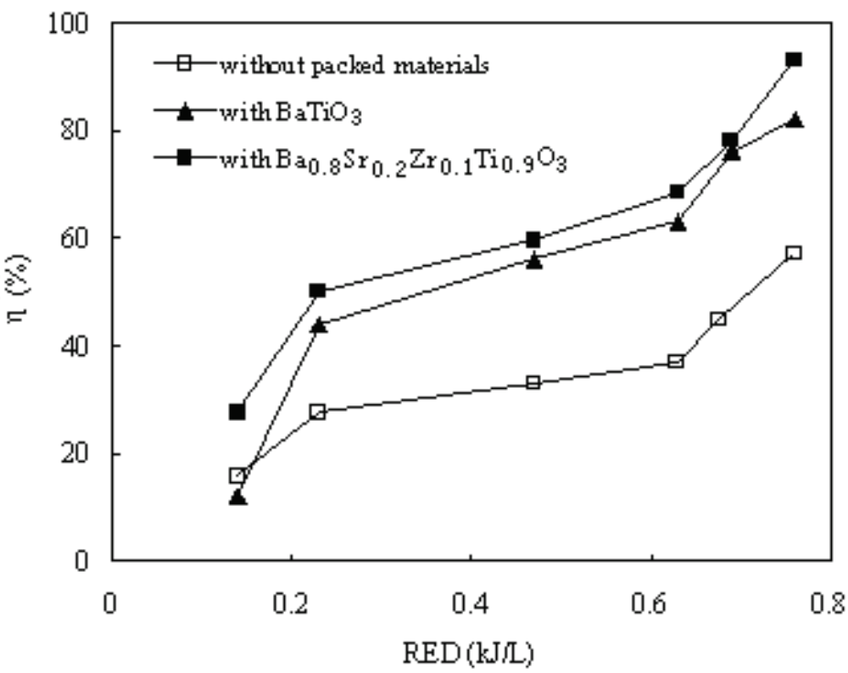

Fig. 10. Effect of packed materials on removal efficiency (toluene concentration: 1000mg/m^3 or so; gas flow rate: 2L/min; AC frequency: 150Hz)

The influence on toluene removal efficiency of some other parameters than could be taking into account such as the permittivity of packed materials, surface specific area, adsorption properties or catalytic effect:

1. It is well known that the presence of solid material in the electrode gap enhances the NTP efficiency likely by favoring the formation of homogeneous plasma rather than a filamentous one. Eliasson et al. reported that the packed materials in NTP reactors played a key role for the proper functioning of DBD and generating more high energy electrons. As the removal efficiency was proportional to the numbers of high energy electrons, because these high energy electrons could destroy the molecular structure of toluene and decompose toluene molecules into CO_2, CO and H_2O by effective collisions taking place between the high energy electrons and the toluene molecules.
2. $Ba_{0.8}Sr_{0.2}Zr_{0.1}Ti_{0.9}O_3$ has higher permittivity than $BaTiO_3$. The electric field strength is positive to the permittivity of packed materials in the NTP reactor.
3. It is well known that the surface specific area is positive to the adsorption properties of the adsorbent. The rings of $BaTiO_3$ and $Ba_{0.8}Sr_{0.2}Zr_{0.1}Ti_{0.9}O_3$ have bigger surface specific area of 59 and 57 or so after the rings are calcined at 1200℃. The adsorption properties can adsorb radicals to accelerate decomposition reaction on the surface of the sorbent and the surface of the cellular rings can also become active sites with electrons striking. So the NTP reactor with packed materials can obtain higher toluene removal efficiency than that without packed materials.

Fig.11 shows the voltage and current waveforms detected by oscillograph with and without packed materials ($Ba_{0.8}Sr_{0.2}Zr_{0.1}Ti_{0.9}O_3$ rings) at electric field strength of 10 kV/cm. Ricketts et al.[16] believed that the pulse peak numbers of gas discharge were directly proportion to the removal efficiency of VOCs. As shown in figure 6, the pulse peak numbers are higher with packed materials than those without in the NTP reactor. So packed materials increase the pulse peak numbers of DBD and help for increasing the removal efficiency.

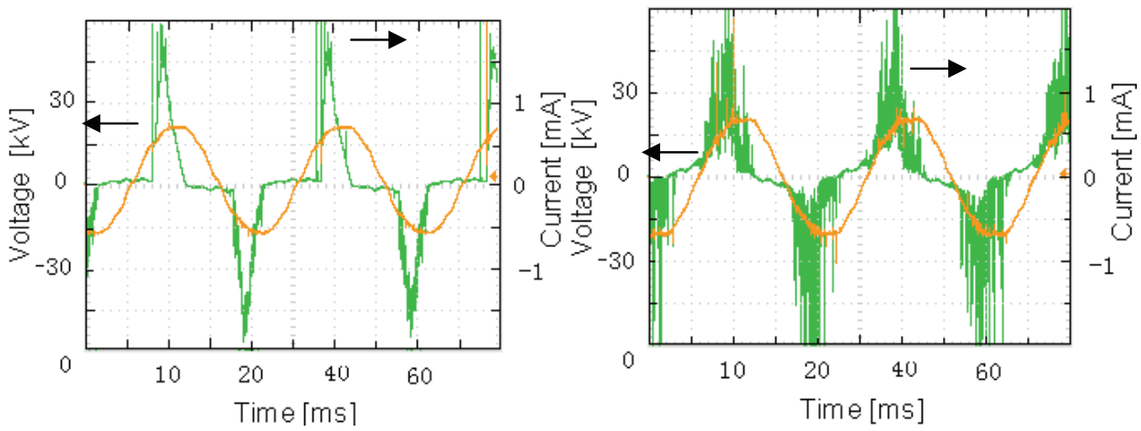

(a) Without packed materials: (b) With packed materials:

Fig. 11. Voltage and current waveforms

Fig.12 shows V-Q Lissajous diagram with or without packed materials ($Ba_{0.8}Sr_{0.2}Zr_{0.1}Ti_{0.9}O_3$ rings) at electric field strength of 10 kV/cm. BC and AD shown in fig.12 represent DBD courses. The packed materials enhance the discharge intensity of BC and AD courses and

produce higher the pulse peak numbers. Pulse peak numbers are directly proportion to RED and increase the removal efficiency of toluene.

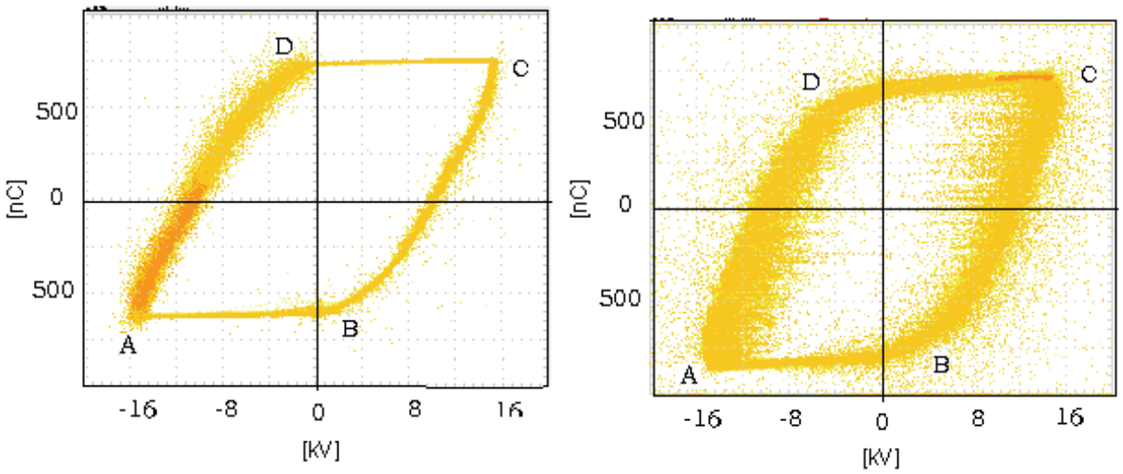

(a) Without packed materials: (b) With packed materials

Fig. 12. V-Q Lissajous diagram

Therefore, the removal efficiency was higher with packed materials than that without packed materials, in agreement with the results shown in fig.10. During the preparation of $Ba_{0.8}Sr_{0.2}Zr_{0.1}Ti_{0.9}O_3$ sample, strontium (Sr) and zirconium (Zr) ions were adulterated into the powder particles and crystal boundary. These metal ions enter crystal lattices of $BaTiO_3$ equably and lower the Curie temperature (Tc). As a result, the permittivity of $Ba_{0.8}Sr_{0.2}Zr_{0.1}Ti_{0.9}O_3$ is 12000, 8 times higher than that of pure phase of $BaTiO_3$ (1500) in room temperature. According to Yamamoto et al., the dielectric constant had a significant influence on the discharge energy of the NTP reactor. The electric field strength is calculated as follows:

$$E_r = \frac{3\varepsilon}{\varepsilon + 2} E_0 \cos\theta \tag{19}$$

Where E_r is the local electric field strength after dielectric polarization, E_0 the local electric field strength before dielectric polarization, and ε the relatively permittivity. As shown in formula (19), E_r is in direct ratio with E_0. E_r equals to 3 times of E_0 (θ=0) with ε close to infinity. So, the electric field strength is positive to the relative permittivity of packed materials in the NTP reactor. RED increases with the electric field strength, improving the removal efficiency of toluene. Therefore, $Ba_{0.8}Sr_{0.2}Zr_{0.1}Ti_{0.9}O_3$ leads to better the removal efficiency of 97% for toluene decomposition.

3.4 Effect of $Ba_{0.8}Sr_{0.2}Zr_{0.1}Ti_{0.9}O_3$ on energy efficiency

Fig.13 shows the change of energy efficiency (ζ) for toluene removal with and without the packed materials. At the identical RED, the energy efficiency is in the order of without packed materials < with $BaTiO_3$ < with $Ba_{0.8}Sr_{0.2}Zr_{0.1}Ti_{0.9}O_3$. The energy efficiency is 15 g/kWh with $Ba_{0.8}Sr_{0.2}Zr_{0.1}Ti_{0.9}O_3$, 11 g/kWh with $BaTiO_3$, and 6 g/kWh without packed materials at RED of 0.23 kJ/L in the NTP reactor. The results show that $Ba_{0.8}Sr_{0.2}Zr_{0.1}Ti_{0.9}O_3$

has a better ferroelectric property to improve energy efficiency and reduce energy consumption in the NTP process for VOCs control, compared with $BaTiO_3$.

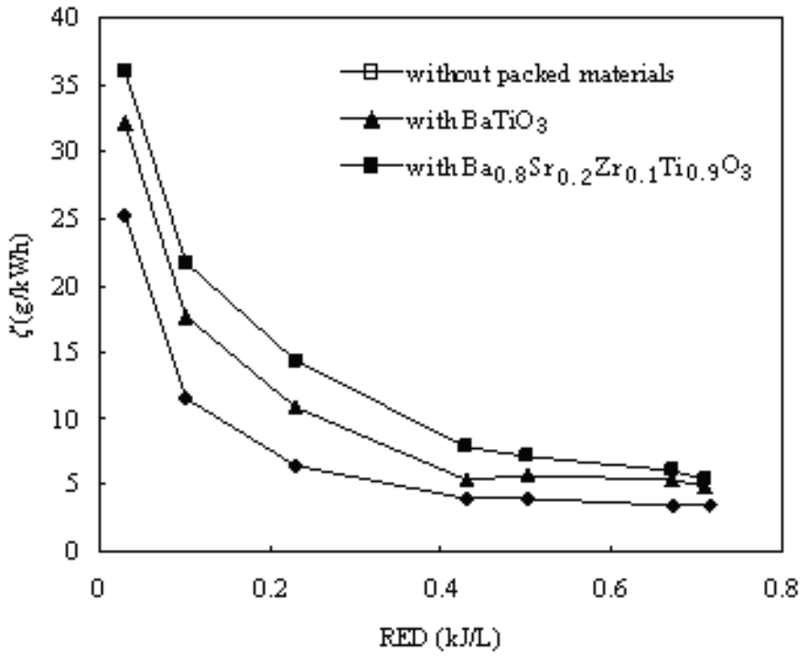

Fig. 13. Effect of packed materials on energy efficiency (toluene concentration: 1000mg/m^3 or so; gas flow rate: 2L/min; AC frequency: 150Hz)

3.5 Effect of $Ba_{0.8}Sr_{0.2}Zr_{0.1}Ti_{0.9}O_3$ on ozone formation

Fig.14 shows the ozone (O_3) concentration with and without the packed materials. O_3 concentration is the highest with $Ba_{0.8}Sr_{0.2}Zr_{0.1}Ti_{0.9}O_3$ and is in the order of without the packed materials < with $BaTiO_3$ < with $Ba_{0.8}Sr_{0.2}Zr_{0.1}Ti_{0.9}O_3$ at the identical RED.

O_3 as the main long-living radical was generated and transported to the packed materials and could take part in oxidation reaction on the packed materials' surface. The pathways of reaction were stated as follows:

$$e + O_2 \rightarrow 2O + e \tag{20}$$

$$O + O_2 + M \rightarrow O_3 + M \tag{21}$$

$$O + O_3 \rightarrow 2O_2 \tag{22}$$

$$e + O_3 \rightarrow O + O_2 + e \tag{23}$$

In figure 9, it also shows that O_3 concentration increases with the REDs at the first stage from 0 to 0.7 kJ/L and reaches the maximum at the RED of 7 kJ/L or so. This pattern of ozone production had also been reported by Yamamoto et al. In this experiment, because $Ba_{0.8}Sr_{0.2}Zr_{0.1}Ti_{0.9}O_3$ has higher relative permittivity than $BaTiO_3$, the electric field strength and RED are enhanced significantly in the NTP process with $Ba_{0.8}Sr_{0.2}Zr_{0.1}Ti_{0.9}O_3$ as the

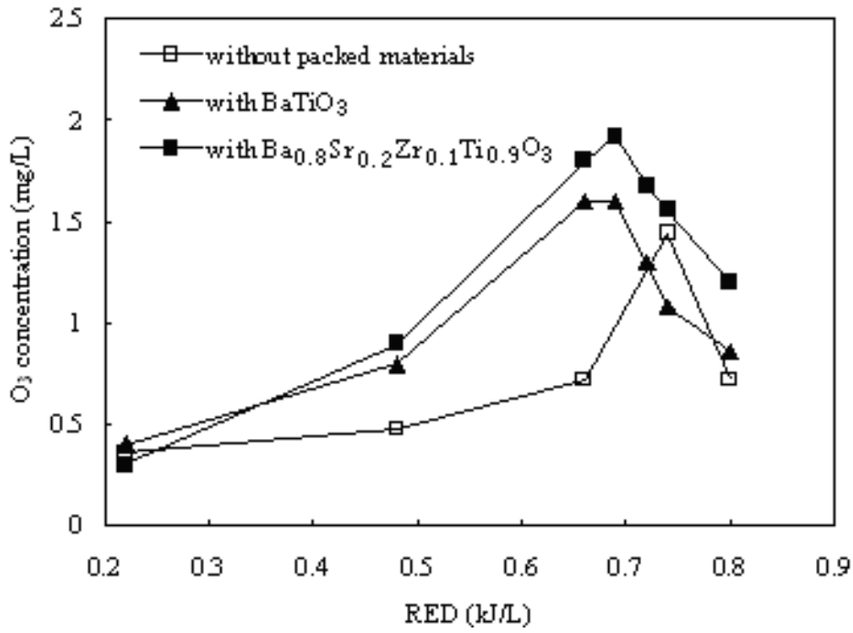

Fig. 14. Effect of packed materials on O_3 concentration (toluene concentration: 1000mg/m^3 or so; gas flow rate: 2L/min; AC frequency: 150Hz)

packed materials. As a result, O_3 concentration increases according to Equation (21) (RED ≤ 0.7 kJ/L). While RED ≥ 0.7 kJ/L, the superfluous high-energy electrons accelerate the decomposition of O_3 to O_2 according to Equation (22) and Equation (23). The active oxygen species formed during the O_3 decomposition would also be helpful for the toluene removal on the surface of packed materials.

4. Decomposition of benzene in dry air by super-imposed barrier Discharge NonThermal plasma–photocatalytic system

In this section, NTP coupled with nano-titania (TiO_2) photo-catalyst for benzene decomposition to further reducing the energy consumption and harmful byproducts in plasma process.

O_2 and H_2O are adsorbed on the surface of TiO_2 to form adsorption oxygen and adsorption water:

$$O_2(g) \rightarrow O_2(ads) \tag{24}$$

$$H_2O(g) \rightarrow H_2O(ads) \tag{25}$$

The molecules of VOC are also adsorbed on the surface of TiO_2 to form adsorption matter:

$$VOCs \rightarrow (VOCs)_{ads} \tag{26}$$

Discharge plasma as a driving force of photocatalyst furnished a mess of UV light. According to Kim's report, hole-electron pairs are produced by supplying energy larger than the band-gap energy of TiO_2 (3.2 eV for anatase crystal type).

$$TiO_2 + h\nu \rightarrow TiO_2(e^- + h^+) \tag{27}$$

And then, OH radicals come into being:

$$h^+ + H_2O(ads) \rightarrow {}^{\bullet}OH + H^+ \tag{28}$$

$$h^+ + OH^- \rightarrow {}^{\bullet}OH \tag{29}$$

High-energy particles, such as electrons, excited molecules, and radicals may transfer their energy to TiO_2 by bombardment when TiO_2 is placed in a NTP reactor. Various chemical reactions are induced on the excited TiO_2 surface through the following reactions:

$$e^- + O_2(ads) \rightarrow {}^{\bullet}O_2^-(ads) \tag{30}$$

$${}^{\bullet}O_2^-(ads) + H^+ \rightarrow HO_2^{\bullet} \tag{31}$$

$$2HO_2^{\bullet} \rightarrow O_2 + H_2O_2 \tag{32}$$

$$H_2O_2 + {}^{\bullet}O_2^-(ads) \rightarrow {}^{\bullet}OH + OH^- + O_2 \tag{33}$$

At last, the molecules of VOC are decomposed as follow:

$${}^{\bullet}OH_{ads}(HO_{2ads}^{\bullet}, O_{ads} \text{ or } h^+, \text{etc.}) + (VOCs)_{ads} \rightarrow (\text{active intermediate products}) \rightarrow\rightarrow CO_2 + H_2O + CO \tag{34}$$

This section illuminates the experimental results of the effect of packed materials on benzene decomposition using NTP generated by dielectric barrier discharge (DBD) coupled with nano-TiO_2 catalyst. The effects of A and B packed materials on benzene removal were compared in the paper. The results show that removal effect was visible by B packed materials in NTP reactor. At the same time, we got higher removal efficiency and a better selectivity of carbon dioxide or carbon monoxide with B packed materials coated with nano-TiO_2. Above all that means this technology of self-support ray polarization would have a great potential for application in the future.

4.1 Materials and methods

There are two kinds of packed materials of A and B (i.d.2, 4, 5, 7 mm, thickness 3 mm, length 10 mm, raschig ceramic ring) in NTP reactor. The structure characteristics of packed materials A and B were detected by XRD as shown in fig.15 (manufactured by Japan, D/MAX-RA). According to fig.15, the results of physics characteristic of two packed materials were indicated in tab.1. Non-crystal content of A packed materials was up to 70% and non-crystal content of B packed materials was 50%. It means B packed materials interstitial rate was higher than A packed materials, and adsorption capability was bigger than A packed materials.

The packed materials coated with nano-TiO_2 catalyst were packed into the reactor. The reactor was made of ceramic tube (i.d.50 mm, reaction length 500 mm), inner axes electrode (i.d.0.8 mm, stainless steel wire), and outer electrode (80 circles stainless steel wire). The characteristic of packed materials includes volume density is 21.7 g/cm^3, hole rate is 12.7 % and bibulous is 5.9 %.

Packed materials	Component（%）			Interstitial rate（%）	Hygroscopic coefficient（%）
	quartz	Al_2O_3	non-crystal		
A	15	15	70	1.8	0.8
B	15	35	50	19.5	9.4

Table 1. Physics characteristic of two packed materials

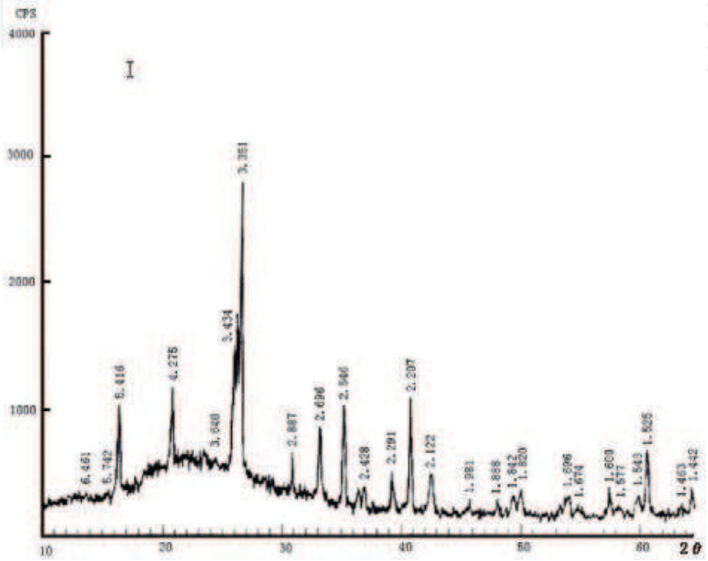

(a) A packed materials

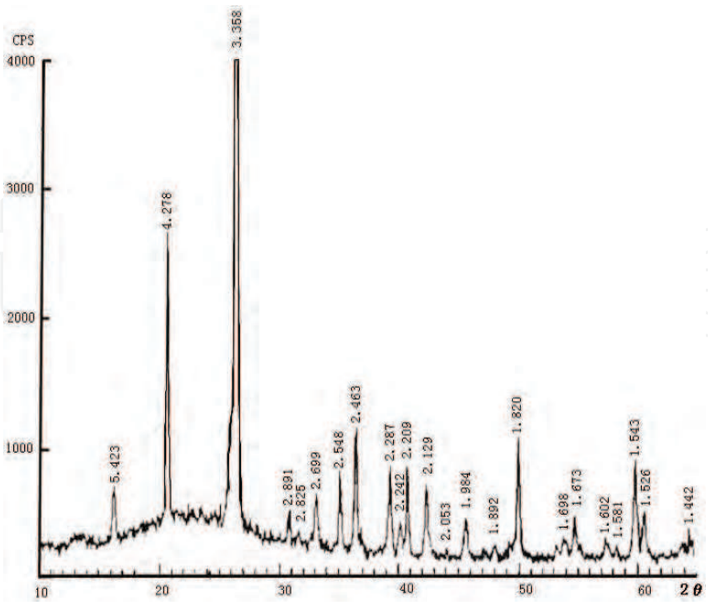

(b) B packed materials

Fig. 15. XRD pattern of packed materials

Nano-TiO_2 films were prepared by the Sol-Gel method in the experiment. Flow chart on preparing nano-TiO_2 thin film by Sol-Gel method referred to Fig.16.

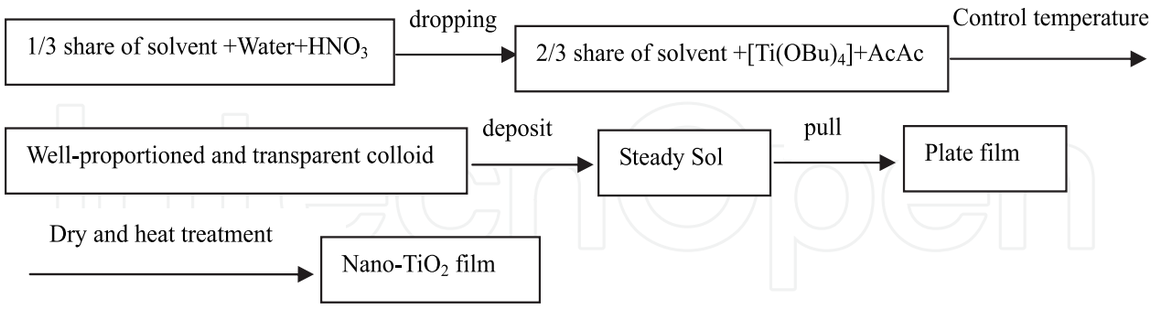

Fig. 16. Flow chart on preparing nano-TiO_2 thin film by Sol-Gel method

The nanometer TiO_2 thin film was inspected and analyzed by Scan Electric Mirror (SEM, Made in Japan, S-2700). The results of SEM micrograph show that average particulate diameters of TiO_2 were less than 100 nm. SEM micrograph of the samples referred to Fig.17.

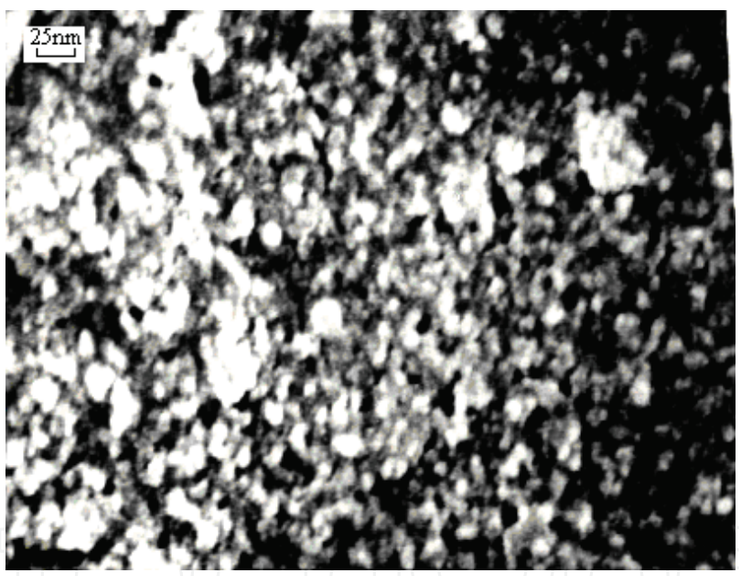

Fig. 17. SEM micrograph of TiO_2

The plasma reactor employed an alternating current (AC) power supply of 60 Hz (designed by ourselves). The AC voltage was applied to the reactor in the radial direction, and the AC voltage extension lied from 0 kV to 30 kV. The benzene concentration was determined on a gas chromatography (manufactured by American Thermo Finnegan Co., TRACE-GC ULTRA) with a flame ionization detector (FID) and a capillary column of DB-1. Separately, another GC (SC—1001) equipped with an FID detector and a methane converter was used to analyze concentration of CO_2 and CO. Reaction gas samples were taken by a syringe from the sampling ports of the reactor. The byproducts were identified by GC-MS with a 30-m-long wide–bore capillary column (DB-1). The experimental condition was in atmospheric pressure (760 mmHg) and temperature (20℃).

4.2 Relationship packed materials between and removal efficiency

Fig.18 & Fig.19 showed the effect of A & B packed materials on removal efficiency of benzene (benzene concentration of 600 mg/m^3, gas flux is 100 L/h, dry air, A & B packed materials coated with nano-TiO_2). With increasing electric field strength, the removal efficiency of benzene increased. During an impulse cycle in NTP reactor, a mass of high-energy electrons were produced in discharge space. When effective collisions between high energy electrons and benzene molecules took place in NTP reactor, electron energy would destruct molecular structure of benzene and benzene molecules could be converted into inorganic little molecules like carbon dioxide (CO_2), carbon monoxide (CO) and water (H_2O) at last. Thus, removal efficiency of benzene was proportional to the number of electrons, while the electrons' number was positive to electric field strength. It had come to light that TiO_2 was helpful for generating higher concentrations of different types of active oxygen species in non-thermal plasma. So the hybrid system would have an effective utilization of active oxygen species in benzene removal.

As shown in fig.18, removal efficiency with B packed materials (i.d.2 mm) was higher than that with A packed materials (i.d.2 mm). Firstly, compared with the component of A & B packed materials, non-crystal type being in existence had influence on dielectric polarization. Secondly, B packed materials possessed higher interstitial rate and hygroscopic coefficient and bigger surface area. These factors were helpful for benzene molecule adsorption so that they prolonged reaction time between benzene molecule and high electrons or free radicals. Thirdly, the surface of B packed materials was rough and could assemble more polarization electric charge to form more local electric field, so that electrons in NTP gained higher energy to improve reaction efficiency.

As shown in fig.19, the size of B packed materials (i.d.2, 4, 5, 7 mm) had effect on removal efficiency of benzene. Removal efficiency increased with the size of raschig ceramic ring decreasing. The removal efficiency was an order of i.d.2 mm > i.d.4 mm > i.d.5 mm > i.d.7 mm. The removal efficiency with B packed materials of i.d.2 mm was 81% with electric field

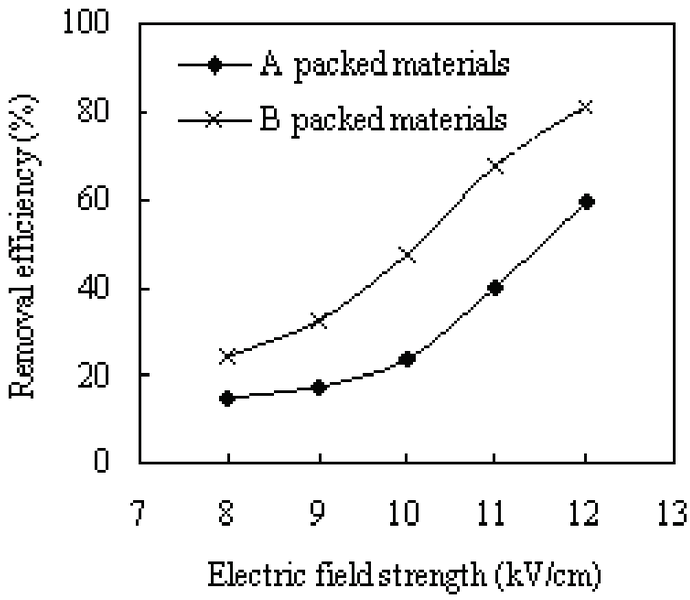

Fig. 18. Effect of different packed materials on removal efficiency

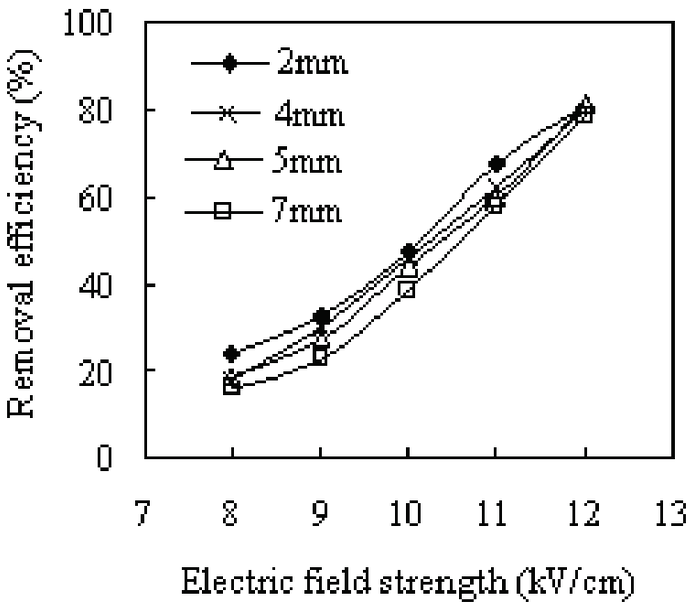

Fig. 19. Effect of different diameters of B packed materials on removal efficiency

strength of 12 kV/cm. With the size of raschig ceramic ring decreasing, packed materials density increased and interspace between packed materials reduced. These factors were helpful for dielectric polarization and enhanced electric field strength. The same result was gained by Ogata *et al*.

4.3 Relationship between packed materials and ozone concentration

Fig.20 and fig.21 showed ozone concentration increased with increasing electric field strength (benzene concentration of 600 mg/m^3, gas flux of 100 L/h, dry air, A & B packed materials coated with nano-TiO_2). When electric field strength increased, more high-energy electrons and radicals were generated in the early discharge phase. They possessed high energy compared to the dissociation energy of O_2 so that a series of reaction took place in NTP reactor. The oxygen dissociation was the most important radical formation reaction.

$$e + O_2 \rightarrow e + O + O \tag{35}$$

Electronically excited atomic oxygen ($O(^1D)$) was a very short-lived radical, whereas ground state atomic oxygen (O) and hydroxyl (OH) had a longer lifetime. $O(^1D)$ reacted with H_2O resulting in formation of OH radicals. O^- and OH^- radicals were consumed by O_3 formation. O_3 as the main long-living radical was transported to packed materials and could take part in oxidation reaction on packed materials' surface. The pathways of reaction were stated as follows:

$$O + O_2 + M \rightarrow O_3 + M \tag{36}$$

$$O + O_3 \rightarrow 2O_2 \tag{37}$$

$$e + O_3 \rightarrow O + O_2 + e\,. \tag{38}$$

As shown in Fig.20, ozone concentration with A packed materials (i.d.2 mm) was higher than that with B packed materials (i.d.2 mm) in NTP reactor. Because the adsorption capability of B packed materials in NTP reactor was higher than that of A packed materials. It meant B packed materials would be helpful for decreasing ozone concentration though prolonging reaction time on the surface of B packed materials followed equation (37) to (38). As shown in fig.21, ozone concentration was an order of B packed materials of i.d.2 mm > i.d.3 mm > i.d.5 mm > no padding. It was obvious that B packed materials was helpful for increasing ozone concentration. The reaction took place just like equation (36).

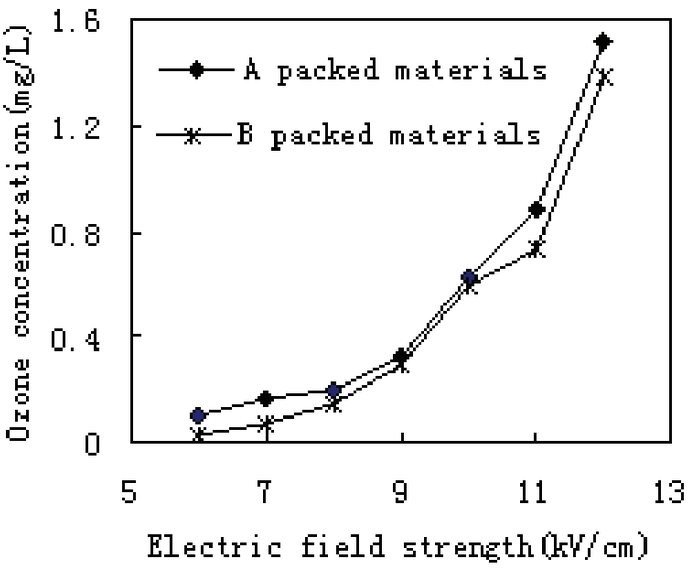

Fig. 20. Effect of different packed materials on ozone concentration

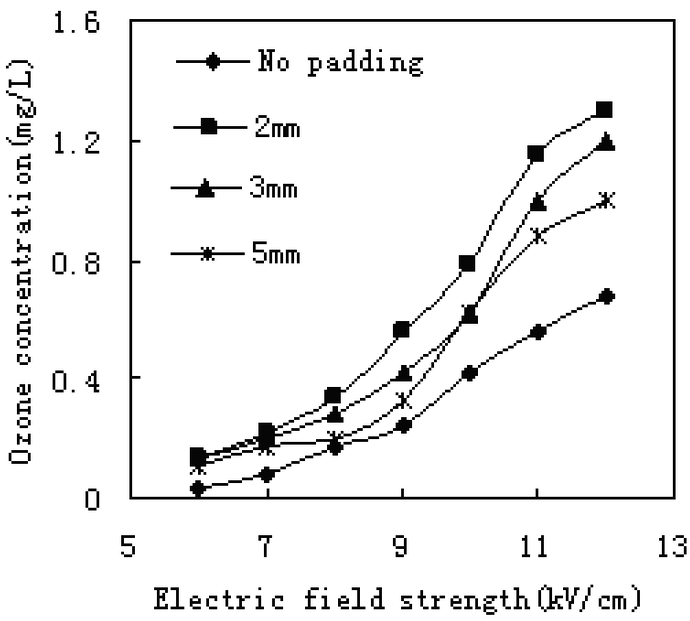

Fig. 21. Effect of different diameters of B packed materials on ozone concentration

4.4 Relationship between power consumption and removal efficiency

Fig.22 showed the biggest electric power consumption was up to 120 W with electric field strength changing from 0 to 12 kV/cm with B packed materials coated with nano-TiO_3. Kuniko Urashima *et al.* got the similar conclusion at the same experimental conditions.

Fig.23 showed that power consumption was 13.5 W if removal efficiency was up to 85% and benzene concentration was 600 mg/m^3. Through calculating, electric energy consumption was 2.25×10^{-4} kWh to treat benzene quality of 1 mg. If benzene concentration was 1500 mg/m^3, power consumption was 20 W for the same removal efficiency. Through calculating, electric energy consumption was 1.33×10^{-4} kWh to treat benzene quality of 1 mg.

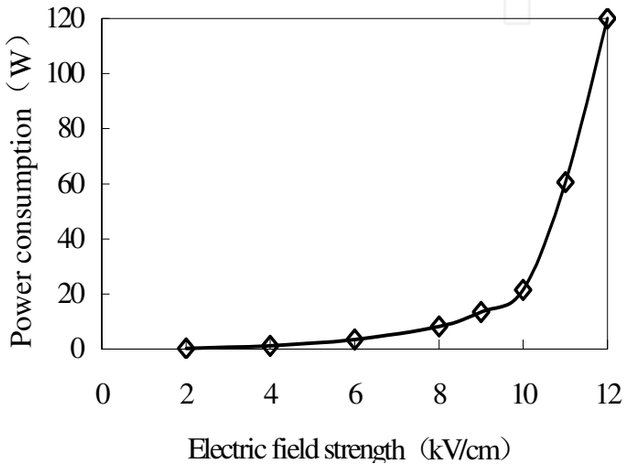

Fig. 22. Relationship between electric field strength and power (B packed materials coated with nano-TiO_2)

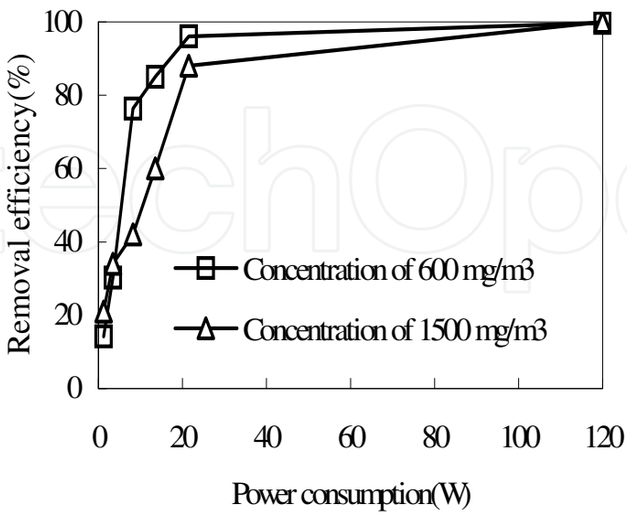

Fig. 23. Relationship between power consumption and removal efficiency (B packed materials coated with nano-TiO_2)

4.5 Photocatalyst and ozone effect

In the next experiment, we chose B packed materials. The packed materials(5 mm i.d., 1 mm wall thick, 10 mm length) were divided into two groups, coated with photocatalyst or without photocatalyst.

Fig.24 shows the relationship between removal efficiency of benzene and electrostatic field strength in the plasma reactor with or without packed materials.

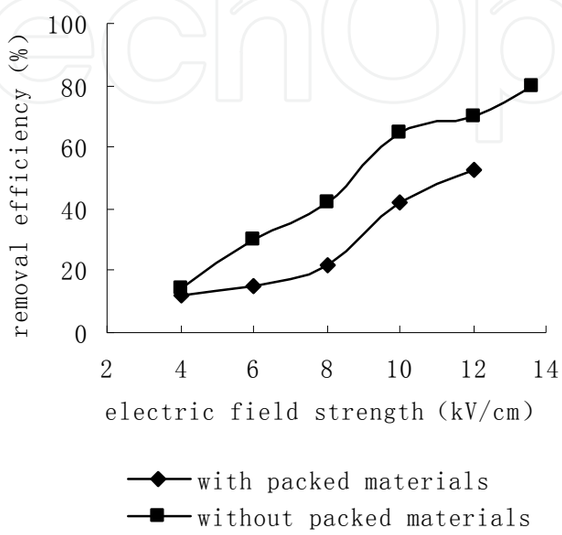

Fig. 24. The effect of removal efficiency with or without packed materials

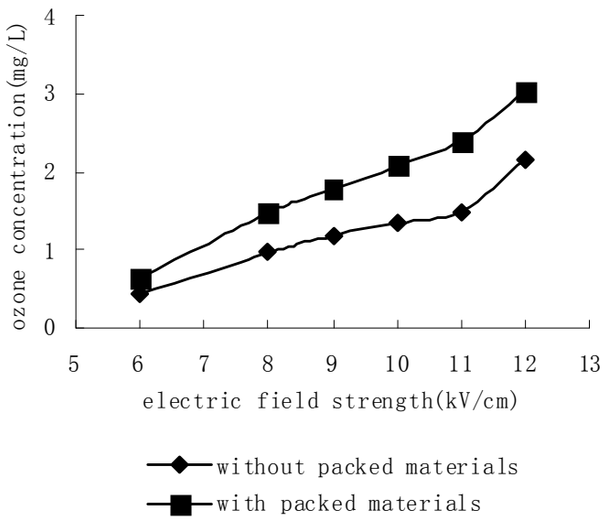

Fig. 25. The effect of ozone concentration with or without packed materials

Fig. 25 shows the relationship between ozone concentration and electrostatic field strength in the plasma reactor with or without packed materials.

With increasing electrostatic field strength, the removal efficiency of benzene increases. When initial concentration of benzene is 1300 mg/m^3, the average electrostatic field strength is 13.6 kV/cm and gas flux is 100 L/h, the removal efficiency of benzene arrives at 80% in the reactor with packed materials as shown in Fig.24.

In the reactor, the space occupied by contamination air is always full of high energy electrons. When effective collisions between high energy electrons and benzene molecules take place in the reactor, electron energy will destruct molecular structure of benzene and benzene molecules will be converted into inorganic little molecules like carbon dioxide (CO_2), carbon monoxide (CO) and water (H_2O). Thus, removal efficiency of benzene are proportional to the electrons. In Fig.3, when packed materials placed in the plasma reactor, with electrostatic field strength increasing, more and more high energy electrons are produced due to mediums polarization of packed materials. So packed materials in the reactor increases the removal efficiency of benzene.

Fig.25 shows when initial concentration of benzene is 1300 mg/m^3, the average electrostatic field strength is 12 kV/cm and gas flux is 100 L/h, ozone concentration is about 3.04 mg/L with packed materials and ozone concentration is about 2.16 mg/L without packed materials. Ozone concentration with packed materials heightens 1 mg/L than that without packed materials in the plasma reactor. It is obvious that packed materials in the reactor is helpful of increasing ozone concentration. The reason is high energy electrons and radicals are generated in the early discharge phase. They possess high energy compared to the dissociation energy of O_2 so that a series of reaction takes place in the plasma. The oxygen dissociation is the most important radical formation reaction.

$$e + O_2 \rightarrow e + O + O \tag{39}$$

Electronically excited atomic oxygen ($O(^1D)$) are very short-lived radicals, whereas ground state atomic oxygen (O) and hydroxyl (OH) have a longer lifetime. $O(^1D)$ reacts with H_2O resulting in formation of OH radicals. O^- and OH^- radicals are removed by formation of O_3.

In Fig.24 and Fig.25, the test results also indicate ozone is helpful for benzene removal, at least, ozone acts as the oxidant precursor. With ozone concentration increasing, the removal efficiency of benzene increases. Because ozone as a kind of oxidative species produced by the initial oxidation just like OH radical, has an effect on further reaction of benzene.

The humidities of contaminated air in the reactor have influence on ozone concentration as shown in Fig.26a. Ozone concentration without vapor is higher 35% than that with relative humidity 67%, and ozone concentration decreases with humidity increasing. Because H_2O molecule have electronegative, it will consume the electrons in the plasma. At the same time, H_2O will react with O (^1D) which is the origin of formation of O_3.

$$H_2O + O(^1D) \rightarrow 2OH \tag{40}$$

So humidity counteracts the formation of ozone.

In Fig.26b, the findings show the removal efficiency reduces with humidity increasing. Probably, the active sites for benzene removal are reduced by water vapor occurring competitive adsorption on the surface of nano-TiO_2.

Thus, humidity affects the benzene removal in three ways: deactivation of high energy electrons, inhibition of ozone formation, and suppression of the catalyst activity of nano-TiO_2 for benzene oxidation with ozone in the plasma reactor.

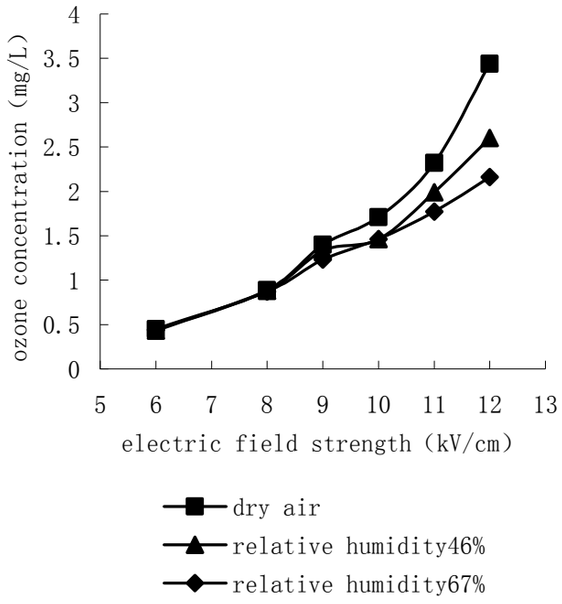

Fig. 26a. The effect of humidity on ozone concentration without photocatalyst

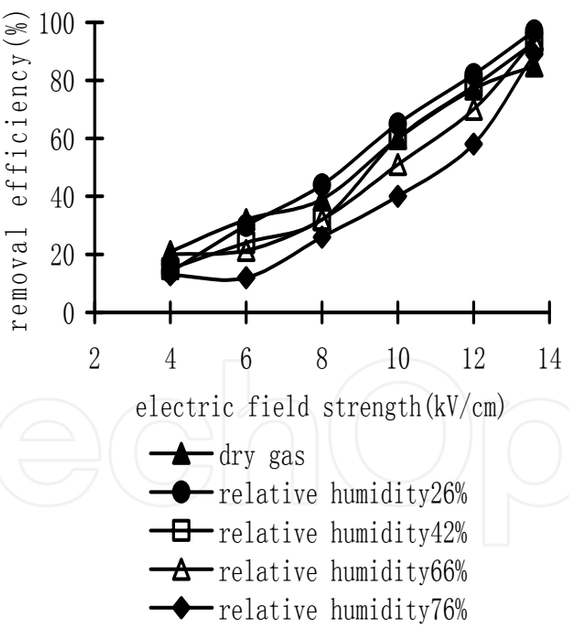

Fig. 26b. The effect of humidity on removal efficiency with photocatalyst

Fig.27 shows the relationship between ozone concentration and gas flux with catalyst or without catalyst in the plasma reactor under three initial concentration of benzene. When gas passes the reactor, and electrostatic field strength is 10kV/cm, ozone concentration increases with gas flux increasing as shown in Fig.27a, 27b and 27c, regardless of with or without photocatalyst.

Fig.27d and 27e show benzene concentration reduces with initial concentration of benzene increasing, regardless of with or without photocatalyst.

The relationship between benzene degradation and electrostatic field strength with or without photocatalyst is shown in Fig.28 where benzene initial concentrations changes from 600 mg/m^3 to 1500 mg/m^3.

When initial concentration is 600 mg/m^3, the average electrostatic field strength is 10 kV/cm, and gas flow rate is 14 mm/s, the removal efficiency of benzene attains 98% in the reactor with photocatalyst, but the removal efficiency of benzene attains 78% in the reactor

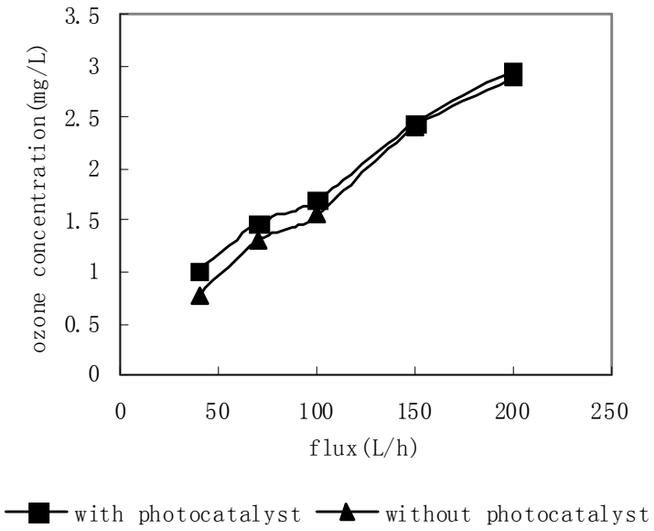

Fig. 27a. Relationship between ozone concentration and flux with or without catalyst when benzene concentration is 0mg/m^3

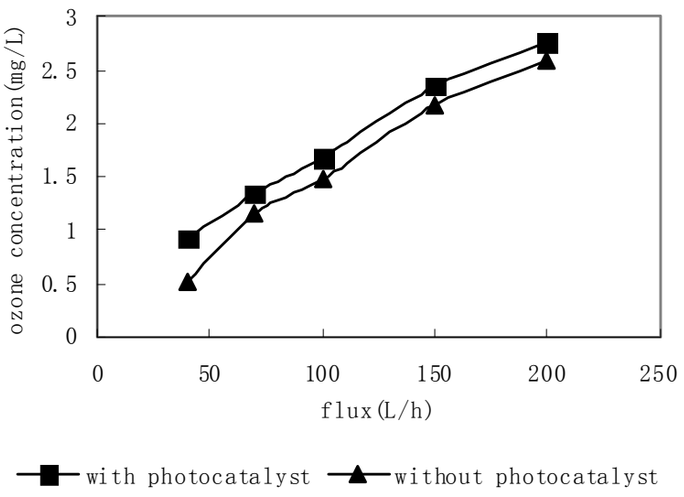

Fig. 27b. Relationship between ozone concentration and flux with or without catalyst when benzene concentration is 700mg/m^3

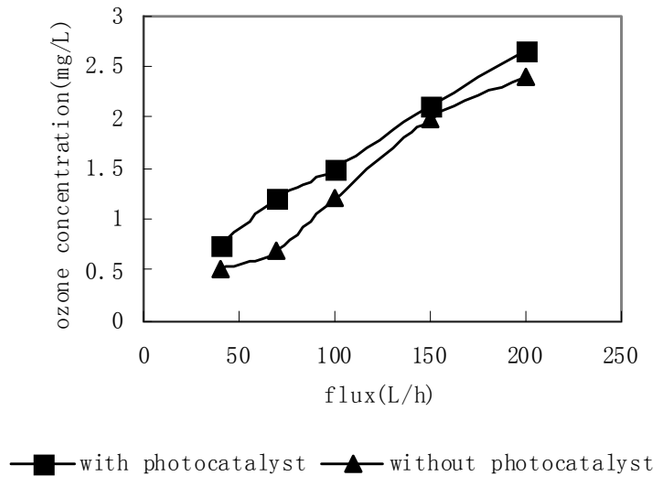

Fig. 27c. Relationship between ozone concentration and flux with or without catalyst when benzene concentration is 2000mg/m^3

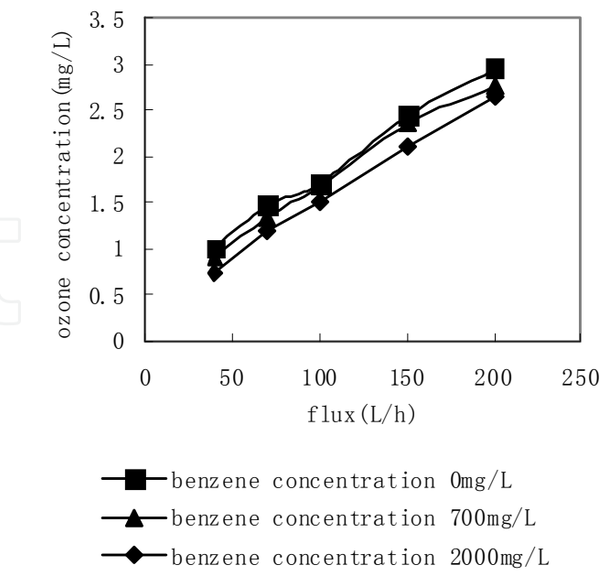

Fig. 27d. Relationship between ozone concentration and flux with catalyst

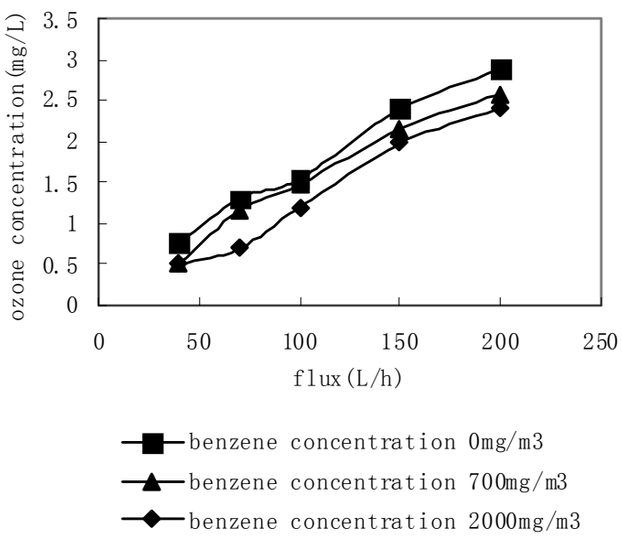

Fig. 27e. Relationship between ozone concentration and flux without catalyst

without photocatalyst as shown in Fig.28a. When initial concentration is 1500 mg/m^3, the average electrostatic field strength is 12 kV/cm and gas flow rate is 14 mm/s, the removal efficiency is higher 19% with photocatalyst than without photocatalyst in the plasma reactor as shown in Fig.28b. The results indicate photocatalyst enhanced the benzene removal efficiency obviously with ozone. When both photocatalyst and ozone coexist, there will be an improved removal efficiency of benzene in the plasma reactor. As you know, TiO_2 is a photocatalyst material of 3.2 eV band gap. If it absorbs bigger energy than band gap, it makes photo-excited electron–hole pairs that could oxidize benzene. At same time, the surface hydroxyl groups are oxidized to form composition of benzene in the photocatalytic reactions. So we have thought that it was advantageous to use photocatalyst in plasma system to control of oxidation step of benzene.

The influence of the catalyst on ozone formation is presented in Fig.27a, 27b and 27c. It shows the catalyst could reduce the ozone formation to a certain extent. This is because ozone as the main long-living radical can capture free electrons which are produced by photocatalysis and produce OH radical. It not only avoids hole-electron pairs compounding but increases photons efficiency. Further more, OH radical is a kind of good oxidant and it can transform organism into mineral.

$$O_3 + e^- \rightarrow O_3^- \bullet \tag{41}$$

$$H^+ + O_3^- \bullet \rightarrow HO_3 \bullet \tag{42}$$

$$HO_3 \bullet \rightarrow O_2 + \bullet OH \tag{43}$$

$$O_3 + hv \rightarrow \bullet O + O_2 \tag{44}$$

$$\bullet O + H_2O \rightarrow 2 \bullet OH \tag{45}$$

From (41)~(45), we can arrive at conclusions. On the one hand, ozone increases photons efficiency of photocatalusis so that is helpful of benzene removal. On the other hand, photocatalyst promotes ozone to separate into OH radical and reduces ozone output.Complete oxidation of benzene to CO_2 is the final goal of the experiment, and the catalytic effect on the product distribution had been investigated. Photo-oxidation activity should be expressed as selectivity to CO_2 because other byproducts except CO_2 were emitted in plasma process.

4.6 The compare of photocatalyzed characteristic by different heat treatment

The packed materials with phot ocatalyst were to calcine at 450ºC, 600ºC and 700ºC in the muffle. Then, they were packed into the plasma reactor. The samples of packed materials were detected by X-Ray and testified that nano-TiO_2 was anatase at 450 ºC and nano-TiO_2 was mixture of anatase and rutileat at 600ºC and nano-TiO_2 was rutile mostly at 700ºC. The experimental results are shown in Fig.28.

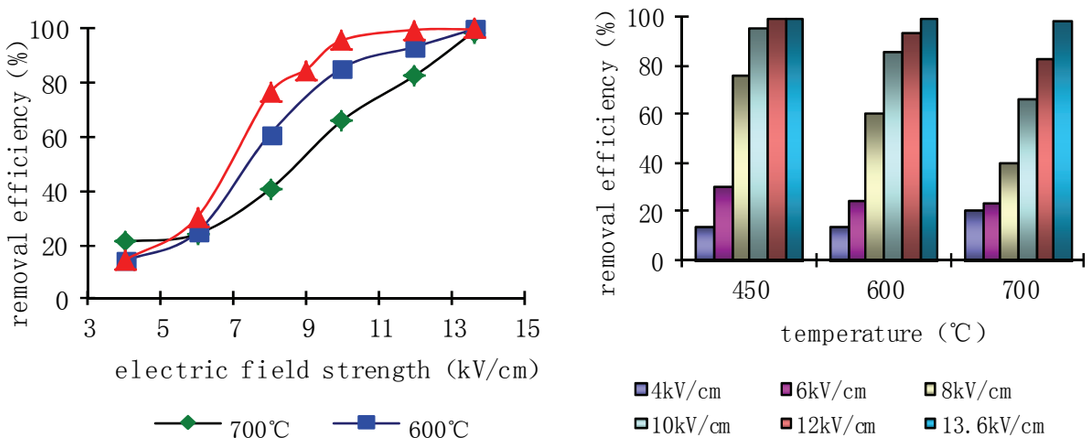

Fig. 28. Compare with catalyst characteristic of different treatment temperature

The decomposition efficiency of benzene is best with anatase photocatalyst in the plasma reactor. Next, the decomposition efficiency is better with the mixture photocatalyst of anatase and rutileat, and the last to rutileat photocatalyst. The above all are shown in Fig.28(a).

Fig.28(b) shows the decomposition efficiency of benzene reduces gradually when the packed materials with photocatalyst by heat treatment from 450ºC to 700 ºC. On one hand, when sinter temperature is raised, the surface areas of catalyst reduce, and the surface adsorption capacity decrease. On the other hand, nano-TiO_2 catalyst will transform from anatase to rutileat. In fig.28(a), the test shows the reaction activity of anatase catalyst is higher than that of rutileat catalyst. There are four reasons.

a. Because of structural difference, two type of catalyst have different quality densities and different structure of energy gap of electron. The quality density of anatase of 3.894g/cm^3 is less than that of rutileat of 4.250g/cm^3. The energy of energy gap of anatase who is 3.2 eV is higher than that of rutileat who is 3.1 eV. The higher energy of energy gap leads to the higher reaction activity for catalyst.

b. The surfaces of anatase possess symmetrical structure with the molecular structure of benzene, so it can adsorb benzene effectively.
c. The hydroxyl of surface of rutileat is not more than that of anatase. Because the hydroxyl of surface is helpful for benzene removal, anatase is better than rutileat on benzene degradation.
d. The surface area of rutileat catalyst declines sharply because a large number of particals converge under high temperature. The adsorption capacity of rutileat of TiO_2 is bad for O_2, so catalyst activity is low.

So nano-TiO_2 photocatalyst of anatase crystal was employed for next experiment.

4.7 Analysis of reaction products

Though GC-MS, the main products in the plasma reactor were CO_2, H_2O, and a small quantity of CO. Ozone was the only byproduct, and no other byproducts could be detected in the tail gas. In addition, certain brown-yellow products that were observed in the plasma reactor regardless of with or without catalyst appeared. The composition of the brown-yellow products was indistinct, and maybe it was aromatic polymer detected by GC-MS.

The minimum of CO/CO_2 is 0.286 and CO/CO_2 decreases with electrostatic field strength increasing as shown in Fig.29a&b. There are no products except CO_2 and H_2O at 11 kV/cm and 12 kV/cm. CO/CO_2 of byproducts is lower 8.2% with catalyst than that without catalyst. These findings show the plasma reactor packed with materials with catalyst has a better selectivity of CO_2 than that without catalyst.

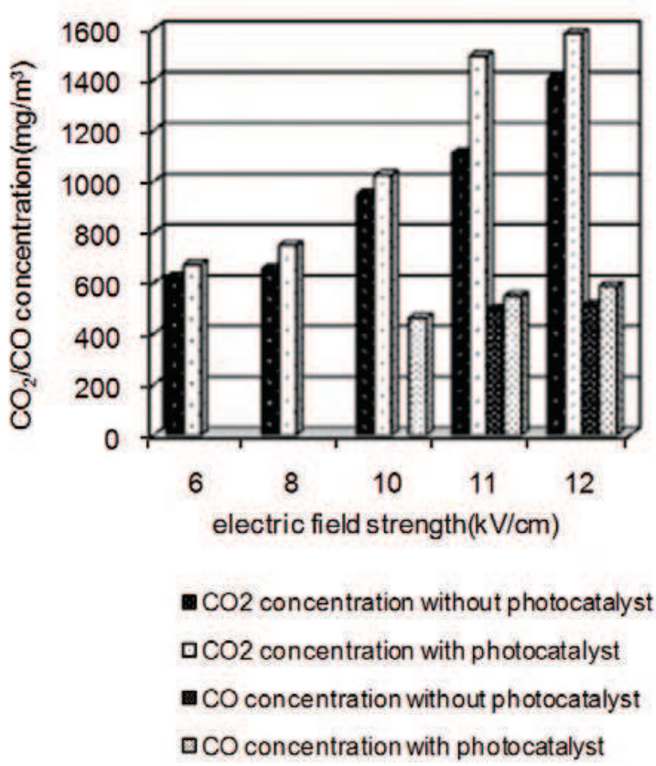

Fig. 29a. Results of byproducts detection when benzene concentration is 750mg/m^3 with or without catalyst

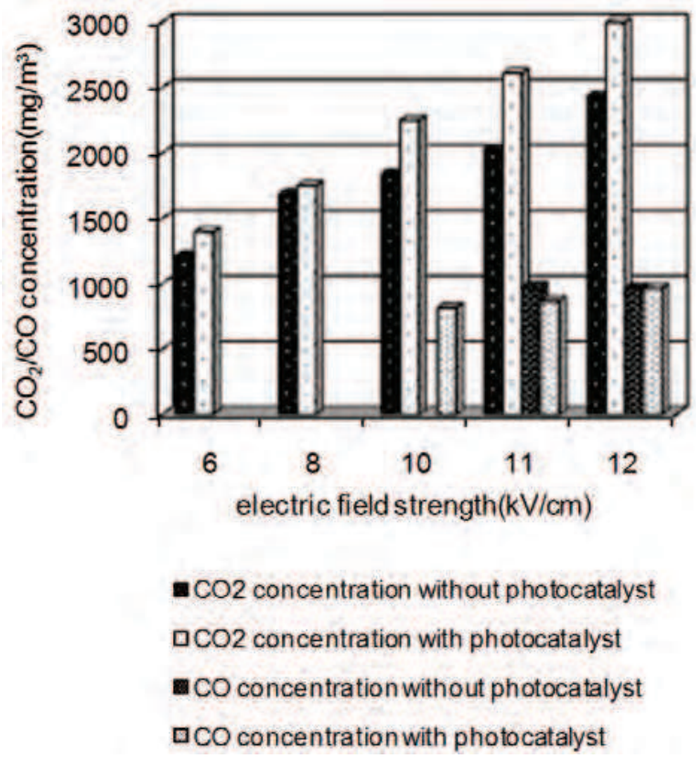

Fig. 29b. Results of byproducts detection when benzene concentration is 1500mg/m^3 with or without catalyst

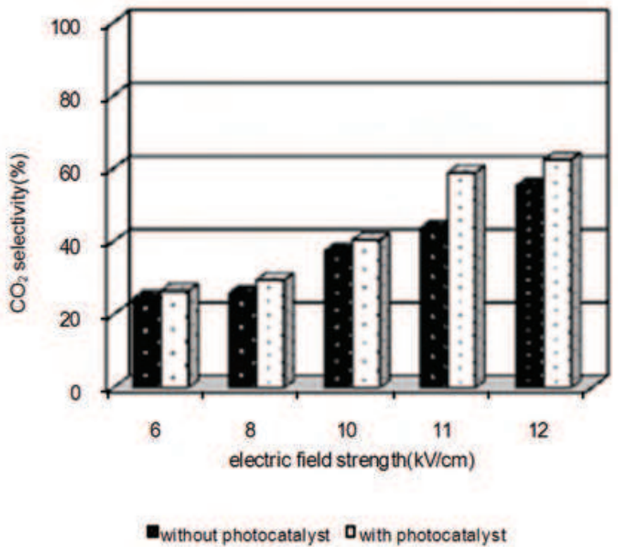

Fig. 29c. CO_2 selectivity when benzene concentration is 750mg/m^3 with or without catalyst

From Fig.29c, it is found the selectivity of CO_2 ranges from 65% to 69% in the plasma reactor without catalyst, while the selectivity of CO_2 ranges from 68% to 73% in the reactor with catalyst. The selectivity of CO_2 is independent of electrostatic field strength. The selectivity of CO_2 is enhanced due to the benzene oxidation near or on the photocatalyst surface. For

that, it could be thought that intermediates and secondary products are more oxidized to CO_2 on photocatalyst surface. With benzene concentration increasing, the total output of CO_2 increases.

Fig.30 showed the change of CO_2 and CO selectivity in NTP reactor with nano-TiO_2 catalyst. The CO_2 and CO selectivity were 61% and 30%, while removal efficiency was 94% at electric field strength of 12 kV/cm, benzene concentration of 1500 mg/m^3 and gas flux of 100 L/h. According to calculating, the total carbon was up to 91%, close to removal efficiency of 94%. It is obvious that NTP coupled with nano-TiO_2 catalyst resulted in a higher CO_2 selectivity and a more thorough removal effect in NTP processing, i.e. the final reaction products were almost CO_2, CO and H_2O.

Fig.31 showed the reaction products detected by GC-MS. According to GC-MS patterns, the main reaction products were CO_2, CO and H_2O, including a very little mass of aldehyde, ketone, acylamide and acetic acid, etc.

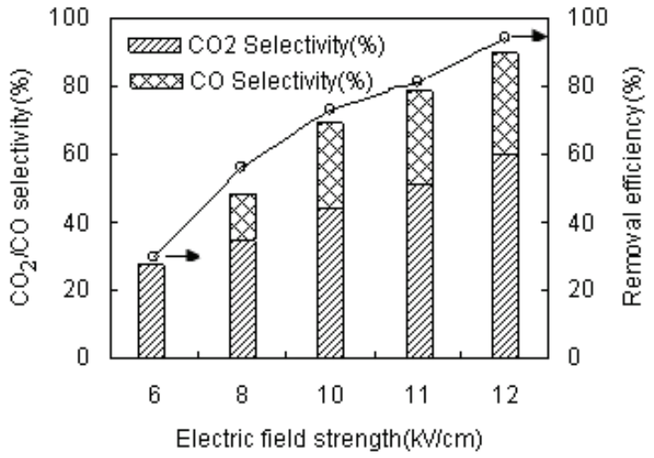

Fig. 30. Relationship between CO_2 and CO selectivity and removal efficiency (B packed materials coupled with nano-TiO_2)

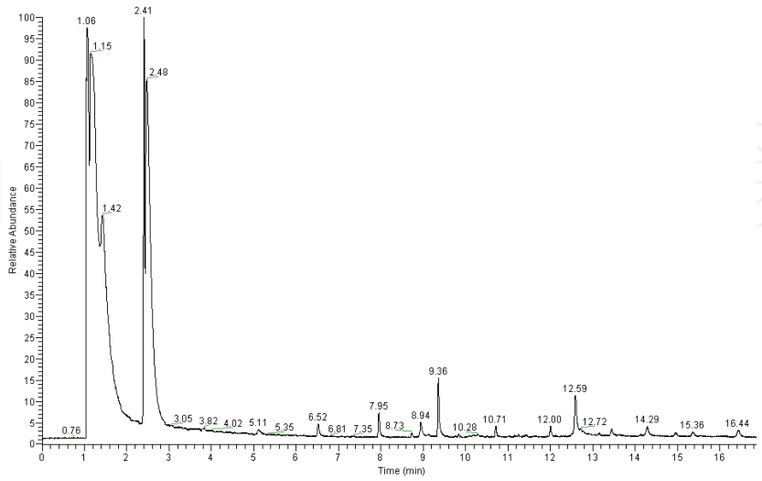

Fig. 31. GC-MS patterns of reaction products (electric field strength of 10 kV/cm, benzene concentration of 1500 mg/m^3, gas flux of 100 L/h, B packed materials of i.d.2 mm coated with nano-TiO_2)

As shown in fig.29-31, the reaction mechanism could be speculated as follows.
Free radicles formation in the surface of nano-TiO_2:

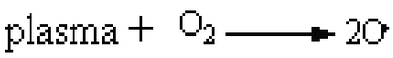
(46)

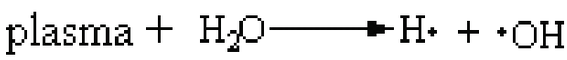
(47)

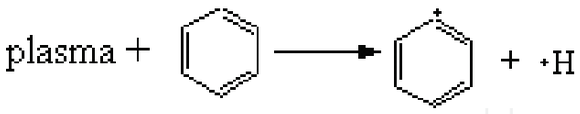
(48)

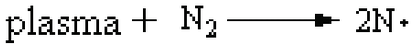
(49)


(50)

The reaction between free radicles and benzene molecules:

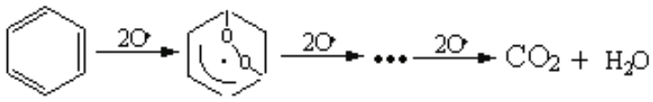
(51)

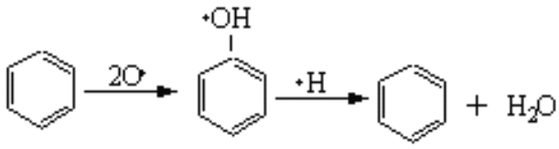
(52)

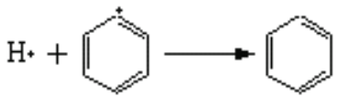
(53)

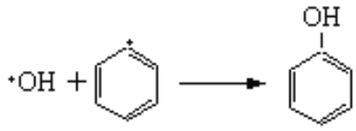
(54)

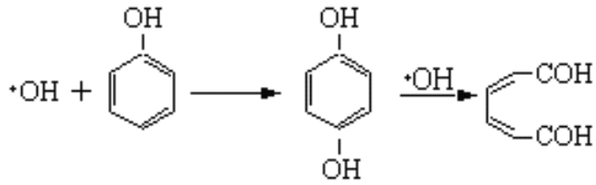
(55)

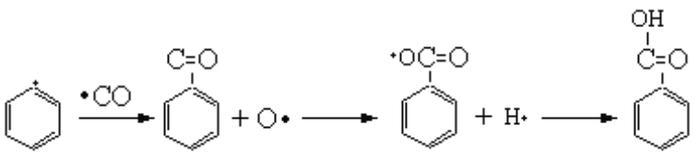
(56)

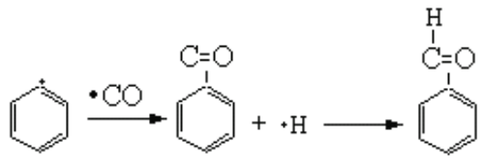
(57)

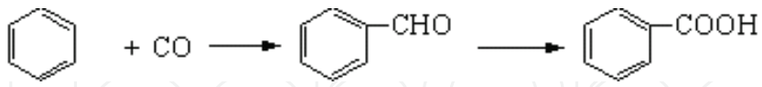
(58)

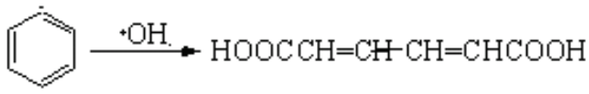
(59)

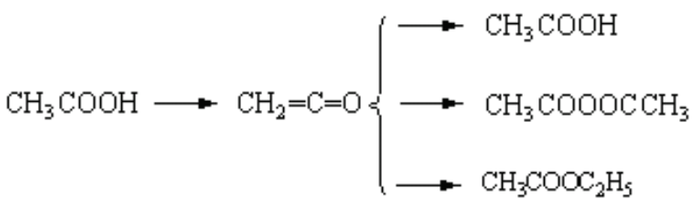
(60)

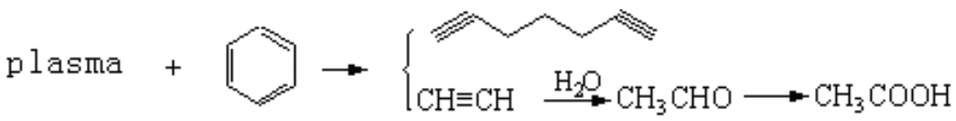
(61)

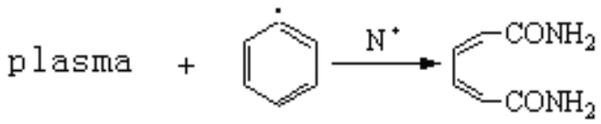
(62)

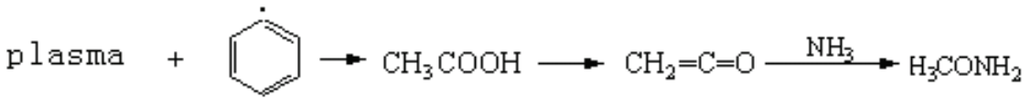
(63)

At last, the final reaction products should be CO_2, CO and H_2O if there was enough energy in NTP reactor from AC high voltage.

5. Synergistic effect of catalyst for oxidation removal of toluene

In our opinion, the best way for removing VOCs is by a combination of plasma and catalytic treatments. Ayrault et al. used platinum (Pt)-based catalyst supported on an alumina wash-coated honeycomb monolith by means of a high voltage bipolar pulsed excitation. The energy removal efficiency of 2-Heptanone was of 0.14 mol/kWh at an energy density of 200 J/L. They also found that energy efficiency decreases to 0.029 mol/kWh when using an uncoated monolith even at an energy density of 500 J/L. Sekiguchi studied degradation of VOCs with an ozone-decomposition catalyst under conditions of UV irradiation. They found that TiO_2 has a lower VOCs removal ratio without UV irradiation and MnO_2-based catalyst has higher VOCs removal ratio at a higher H_2O humidity. MnO_2 is a catalyst for the decomposition of ozone. The researches on the synergistic action of NTP and catalyst have been carried out for more than 10 years, but there are only a few researches, which have

been done adequately, involving byproducts (e.g. O_3) and showing energy efficiency, especially those using MnO_2/γ-Al_2O_3 in AC of 50~500Hz.
In the present work, the synergistic effect of NTP and catalyst for VOCs removal has been studied. It was found that the catalyst could solve the problem of O_3 formation and improve energy efficiency and at the same time increase significantly the removal efficiency of NTP decomposition.

5.1 Materials and methods

VOCs decomposition was studied by using a manganese – alumina catalyst. The manganese catalyst was prepared by intrusion of pellet type alumina, with granule diameter of being 5 – 7 mm and BET (Brunauer Emmett Teller) surface of 228 m^2/g (Detected by Micromeritics, Amercian Quantachrome Co., NOVA 1000).
The specific surface of the catalysts (as determined by the BET method), is given in table 2. BET surface area has not changed too much with catalysts onγ-Al_2O_3.

Catalyst	BET Surface Area(m^2/g)
γ-Al_2O_3	228
TiO_2/γ-Al_2O_3	203
5wt%MnO_2/γ-Al_2O_3	218
10wt%MnO_2/γ-Al_2O_3	202

Table 2. BET surface areas of the catalysts

5.2 Effect of mass percentage of MnO_2 on γ -Al_2O_3

Fig.32 shows the effect of mass percentage of MnO_2 on removal efficiency of VOCs (VOCs concentration: 1000mg/m^3 or so; gas flow rate: 2L/min; AC frequency: 150Hz). The removal efficiency of $MnO_2/\ \gamma$ -Al_2O_3 increased with increasing RED and was of about 10 wt% or 15 wt% >5 wt% at the same RED. However, the removal efficiency of 10 wt% was practically equal to that of 15 wt% at the same RED.
Fig.33 shows the effect of the mass percentage of MnO_2 catalyst in NTP reactor on the concentration of VOCs and ozone in the gas exhaust (RED: 0.5 kJ/L). As the mass percentage of MnO_2 catalyst increased, ozone and VOCs concentrations were diminished, especially in the case of 10 wt% of MnO_2 on γ -Al_2O_3. It is clear that manganese oxides accelerated the decomposition of O_3 to O_2 in gas phase. The active oxygen species formed during the O_3 decomposition must be helpful for VOCs removal by $MnO_2/\ \gamma$ -Al_2O_3.

5.3 Effect of catalyst on removal efficiency and energy efficiency

VOCs removal efficiency is shown in fig.34 as a function of RED with or without TiO_2 or MnO_2 on γ-Al_2O_3. The removal efficiency increased with increasing RED and was in the order of MnO_2/γ-Al_2O_3 > TiO_2/γ-Al_2O_3 > γ-Al_2O_3 at the same RED. It was obvious that MnO_2 and TiO_2 played a role in VOCs oxidation to a certain extent. γ-Al_2O_3 possessed sorbent characteristic, so it could improve VOCs concentration on the catalyst surface and increase the reaction time. MnO_2 is known as metal oxide catalyst and was found to possess a potential activity in redox reactions. MnO_2 surface has been found to expose metal (Mn^{n+}), oxide (O^{2-}) and defect sites of various oxidation states, degrees of coordination unsaturation, and acid and base properties. Furthermore, the d–d electron exchange

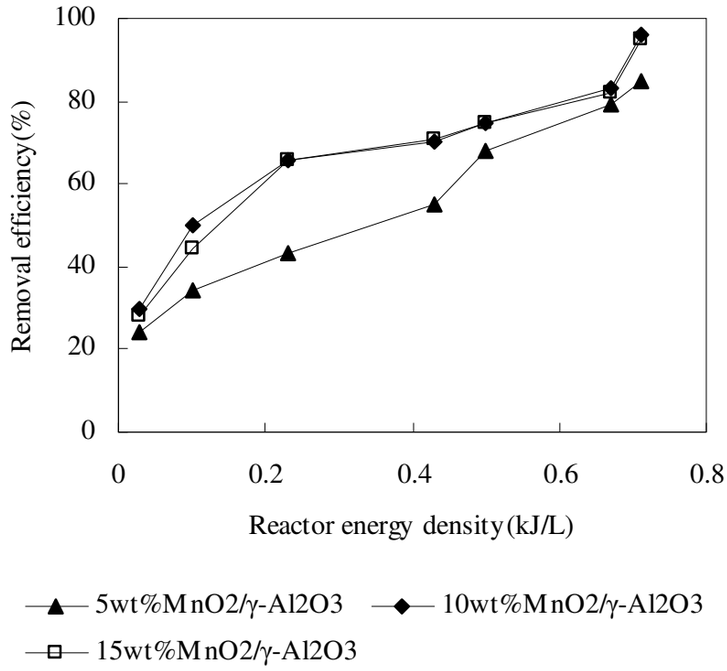

Fig. 32. Effect of mass percentage of MnO_2 on removal efficiency of VOCs

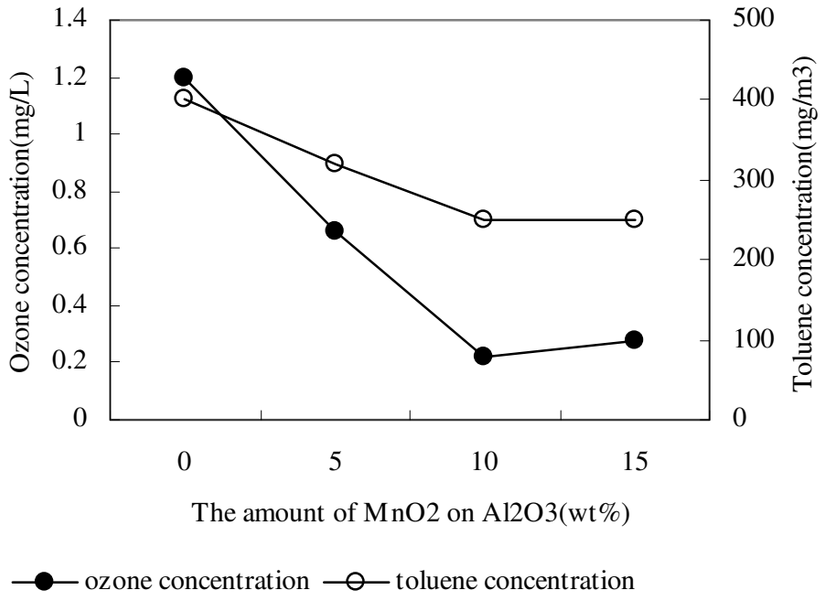

Fig. 33. The changes in the concentration of VOCs and ozone with the amount of MnO_2 on Al_2O_3

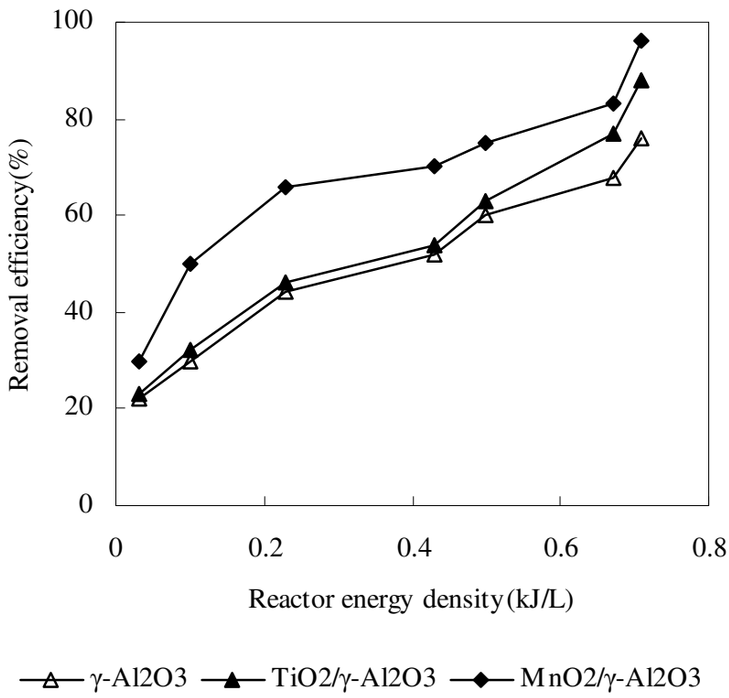

Fig. 34. Effect of RED on removal efficiency with NTP and catalyst combined reactor (10wt% MnO_2/ γ -Al_2O_3; VOCs concentration: 1000mg/m^3 or so; gas flow rate: 2L/min; AC frequency: 150Hz)

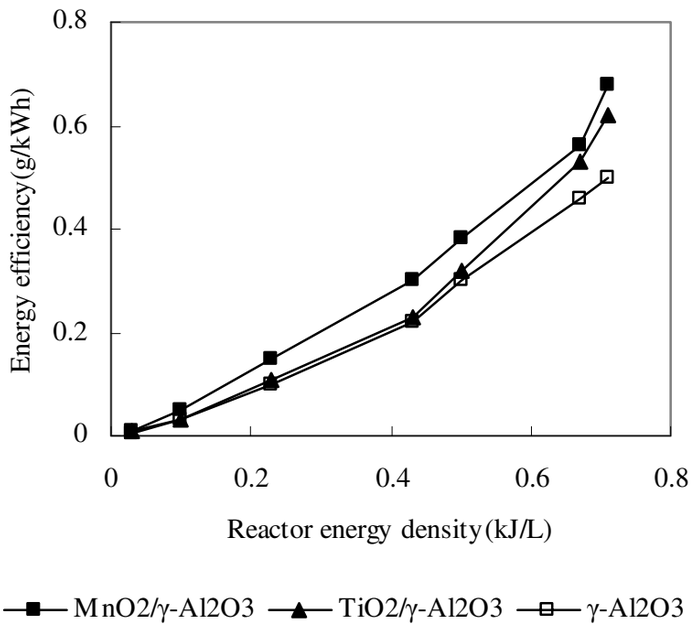

Fig. 35. Relationship between RED and energy efficiency with NTP and catalyst combined reactor (10wt% MnO_2/γ -Al_2O_3; VOCs concentration: 1000mg/m^3 or so; gas flow rate: 2L/min; AC frequency: 150Hz)

interactions between intimately coupled manganese ions of different oxidation states [Mn^{n+}–O–$Mn^{(n+1)+}$] furnish the electron-mobile environment necessary for the surface redox activity. These factors would be helpful for VOCs removal.
At the same experimental conditions, the change of energy efficiency is shown in fig.35. The energy efficiency increased with increasing RED and was in the order of MnO_2/γ-Al_2O_3>TiO_2/γ-Al_2O_3>γ-Al_2O_3 at the same RED. The result indicate that NTP coupled with MnO_2/γ-Al_2O_3 catalyst saved more energy to decompose the same amount of VOCs.

6. Synergistic effect of a combination of catalysts with nonthermal plasma

Many researcher found that for VOCs control, ferroelectric could improve energy efficiency significantly, but ozone concentration increased due to ferroelectric presence. Ogata *et al.* investigated the effects of alumina and metal ions in plasma discharge using NTP reactors packed with a mixture of $BaTiO_3$ and porous Al_2O_3 pellets. The results indicated that the oxidative decomposition of benzene was enhanced by concentrating benzene on the Al_2O_3 pellets. The selected catalyst of MnO_2 was well known for high potentials to decompose ozone. Futamura *et al*. tested catalytic effects of TiO_2 and MnO_2 with NTP. The results showed that the ozone generated from gaseous oxygen is decomposed by MnO_2, but not by TiO_2.
A series of experiments were performed for toluene decomposition from a gaseous influent at normal temperature and atmospheric pressure. In this section, the prepared nano-$Ba_{0.8}Sr_{0.2}Zr_{0.1}Ti_{0.9}O_3$ catalyst was used in the plasma reactor. Doped some ions (Sr & Zr) into the powder particles and crystal boundary in the experiment. The metal ions such as strontium, zinc and zirconium entered into crystal lattices of $BaTiO_3$ equably and the Curie temperature (Tc) fell. As a result, the permittivity of nano-$Ba_{0.8}Sr_{0.2}Zr_{0.1}Ti_{0.9}O_3$ was up to 10^4 which were 12 times higher than that of pure $BaTiO_3$, while dielectric loss reduced to 1/6 in normal temperature. This study found that this nano-material could reduce the energy consumption and increase energy efficiency significantly.
The oxidative decomposition of toluene was enhanced by concentrating toluene on the Al_2O_3 pellets. The selected catalyst of MnO_2 was well known for high potential to decompose ozone. In the experiment, the prepared MnO_2/γ-Al_2O_3 was used as catalyst to reduce the byproducts and toluene concentrations --- also justify about 10 wt%. The objective of this study was to use a combination of catalysts (MnO_2/γ-Al_2O_3 coupled with modified ferroelectric of nano-$Ba_{0.8}Sr_{0.2}Zr_{0.1}Ti_{0.9}O_3$) in the NTP process for toluene decomposition in order to enhance toluene decomposition efficiency and increase energy efficiency and reduce byproducts for commercial applications.

6.1 Materials and methods

An alternating current (AC) of 150 Hz was supplied to the NTP reactor in the radial direction, and the voltage extension changed from 0 kV to 50 kV. The experimental parameters of the process of discharge were detected by an oscillograph (model TDS2014, manufactured by American Tektronix Co.). The primary power values were measured with the voltage-charge（V-Q） Lissajous method in the plasma reactor.
Toluene decomposition was studied with a combination of catalysts including MnO_2/γ-Al_2O_3 and nano-$Ba_{0.8}Sr_{0.2}Zr_{0.1}Ti_{0.9}O_3$ catalysts (volume ratio of 1:1). The manganese oxide catalysts (5wt%, 10wt%, 15wt%) were prepared by impregnation of pellet type γ -alumina with the granules diameter of 5~7 mm and BET surface area of 228 m^2/g detected by Micromeritics (model NOVA 1000, manufactured by American Quantachrome Co.).

Nanometer-sized $Ba_{0.8}Sr_{0.2}Zr_{0.1}Ti_{0.9}O_3$ powders were prepared with inorganic salts, such as $TiCl_4$ and $Ba(OH)_2$, as the raw materials by a water-thermal method at normal pressure. Particulate diameters of $Ba_{0.8}Sr_{0.2}Zr_{0.1}Ti_{0.9}O_3$ was 59 nm which was detected by XRD (model D8 ADVANCE, manufactured by Germany Bruker Co.) and BET surface area was 8.8 m^2/g. The relative permittivity of nano-$Ba_{0.8}Sr_{0.2}Zr_{0.1}Ti_{0.9}O_3$ was about 10^4 (detected by LCR automatism test instrument 4210).

The toluene concentration was determined using a gas chromatography (model HP6890N, manufactured by Agilent Co.) with a flame ionization detector (FID) and a capillary column of HP-5 (internal diameter of 0.32 mm, length 30 m). The byproducts such as aldehyde, alcohols, amide, hydroxybenzene and polymerization products, etc, were identified by GC-MS (manufactured by American Thermo Finnegan Co.) and FT-IR (model Vertex 70, manufactured by Germany). Ozone concentration was measured by a chemical titration method of iodine.

6.2 Effect of combined catalysts on toluene removal efficiency

As the MnO_2/γ-Al_2O_3 catalyst has the best effect for ozone decomposition but not for toluene decomposition, and nano-$Ba_{0.8}Sr_{0.2}Zr_{0.1}Ti_{0.9}O_3$, a type of developmental material on base of pure $BaTiO_3$ (typical ferroelectric), enhances energy efficiency because of its higher relative permittivity of 10^4, a combination of nano-$Ba_{0.8}Sr_{0.2}Zr_{0.1}Ti_{0.9}O_3$ with MnO_2/γ-Al_2O_3 as a combined catalyst was tested in this study.

The effect of various catalysts such as multiple catalyst, nano- $Ba_{0.8}Sr_{0.2}Zr_{0.1}Ti_{0.9}O_3$, MnO_2/γ-Al_2O_3 and no padding on removal efficiency is shown in Fig.36. The removal efficiency increased significantly with the catalysts than that without. The removal efficiency increased in the order of: combined catalyst ＞nano-$Ba_{0.8}Sr_{0.2}Zr_{0.1}Ti_{0.9}O_3$ ＞MnO_2/γ-Al_2O_3 ＞no padding.

The best removal efficiency of 98.7% was achieved in the NTP process. It indicated that the combination of catalysts exhibited a synergistic effect for toluene decomposition.

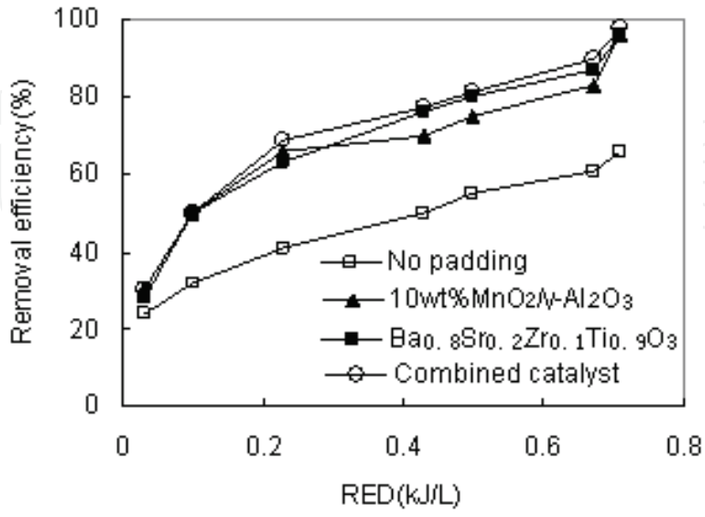

Fig. 36. The change of removal efficiency with various padding (toluene concentration: 800-1000 mg/m^3; gas flow rate: 2 L/min; AC frequency: 150 Hz)

6.3 Effect of combined catalysts on ozone formation

Fig.37 shows the influence of various catalysts on ozone formation with the order of: combined catalyst > MnO_2/γ-Al_2O_3 > no padding > nano-$Ba_{0.8}Sr_{0.2}Zr_{0.1}Ti_{0.9}O_3$ at RED of 0.5 kJ/L. This result suggested that MnO_2/γ-Al_2O_3 in the combination of catalysts should have a main effect on ozone decomposition.

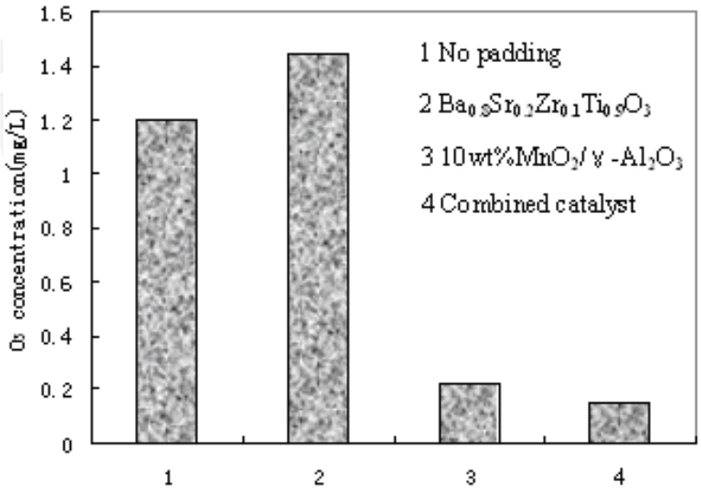

Fig. 37. The change of O_3 concentration with various padding

6.4 Effect of the combination of catalysts on energy efficiency

Fig.38 shows the influence of various catalysts on energy efficiency with the order of: combined catalyst > nano-$Ba_{0.8}Sr_{0.2}Zr_{0.1}Ti_{0.9}O_3$ > MnO_2/γ-Al_2O_3 > no padding at the same SED. These results indicated that the nano-$Ba_{0.8}Sr_{0.2}Zr_{0.1}Ti_{0.9}O_3$ in the combination of catalysts should play an important role for improving energy efficiency.

As a result, the combination of catalysts shows the best removal efficiency of toluene, the best decomposition effect of ozone and the best energy efficiency for toluene removal.

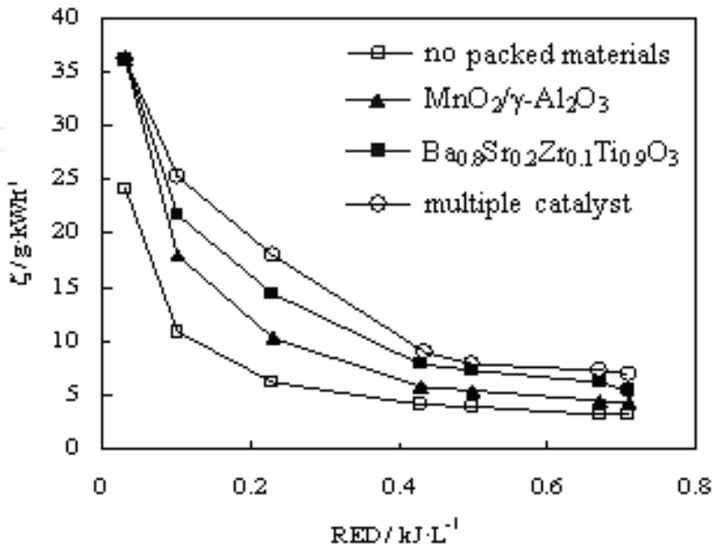

Fig. 38. The energy efficiency with various padding

6.5 Byproducts and decomposition pathways of toluene

Non-thermal plasma has high potential in air cleaning technology, but in some cases unwanted byproducts are formed which could be more harmful than the original VOCs. Fig.39 shows the FT-IR spectrum of the byproducts of toluene decomposition and Fig.40 shows the FT-IR spectrum of the byproducts on the surface of the combination of catalysts.

As shown in Fig.40(a), the -NH- and -NH_2 peak appeared at 3350 cm^{-1} while the peak of 2730 cm^{-1} N=C-N was absent. The peak -NH- with benzene ring appeared at 3450 cm^{-1}, –OH at 3400 cm^{-1}, -CH_3/-CH_2 at 2900 cm^{-1}, benzene derivative (hydroxybenzene, polymerization products, etc) at 1700~1100 cm^{-1}, and CO_2 and CO separately at the rang of 2300~2100 cm^{-1} and 700~500 cm^{-1}. So the byproducts on the surface of the combination of catalysts involved aldehyde, alcohols, amide, and benzene derivative. However, when the combination of catalysts were packed into the NTP reactor, the byproducts on the surface of the packed materials in the NTP reactor reduced greatly as shown in Fig.40(b). Except of amine, CO_2 and CO, no other byproducts were detected on the surface of catalysts. It illuminated that the synergic effect of the NTP with the combination of catalysts could control byproducts effectively.

In Fig.39, the products of toluene decomposition included CO_2, CO and H_2O. At the same time, there are a mass of ozone (strong peak at 1000 cm^{-1}), and several amide and benzene derivatives. Compared spectrum 'a' with 'b' in Fig.39, the benzene derivatives and ozone concentration reduce while the amounts of CO_2 and H_2O increase with the increase of the electric field strength.

A large number of high-energy electrons, ions and free radicals were produced in the NTP reaction process. Firstly, the high-energy electrons could take part in reaction with oxygen in air as follow:

$$\vec{e} + O_2 \rightarrow e + O_2^{\bullet}\,(A^3\textstyle\sum_u^+) \rightarrow e + O(^3P) + O(^3P) \quad (64)$$

$$\vec{e} + O_2 \rightarrow e + O_2^{\bullet}\,(B^3\textstyle\sum_u^-) \rightarrow e + O(^1D) + O(^3P) \quad (65)$$

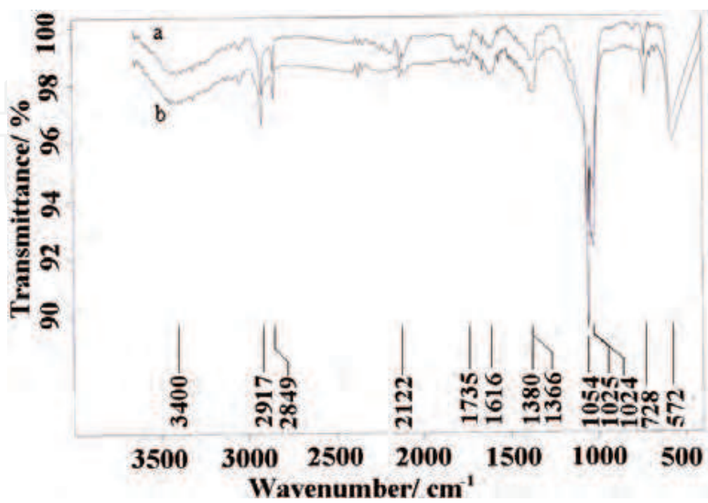

Fig. 39. FT-IR spectrum of the products from toluene decomposition (a. electric field strength of 10 kV/cm; b. electric field strength of 13kV/cm)

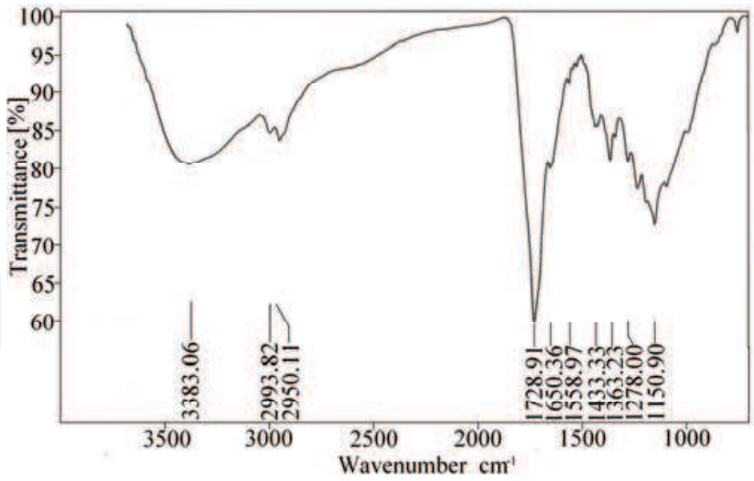

(a) Without catalyst in the NTP reactor

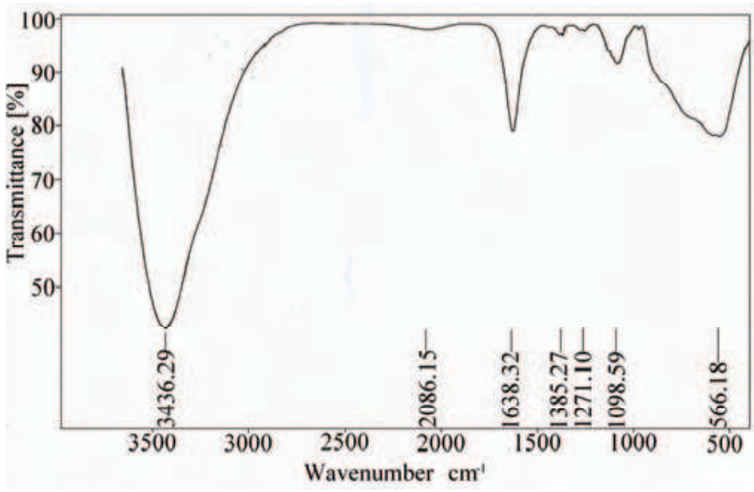

(b) With the combination of catalysts in the NTP reactor

Fig. 40. FT-IR spectrum of the byproducts on the surface of the combination of catalysts

The oxygen free radical groups react with oxygen and other molecules to form ozone:

$$O + O_2 + M \rightarrow O_3^{\bullet} + M \rightarrow O_3 + M \quad (66)$$

At the same time, the high-energy electrons react with H_2O and N_2 in gaseous phase:

$$\vec{e} + H_2O \rightarrow OH^{\bullet} + H^{\bullet} \quad (67)$$

$$\vec{e} + H_2O \rightarrow 2H^{\bullet} + O^{\bullet} \quad (68)$$

$$H_2O + O(^1D) \rightarrow 2OH^{\bullet} \quad (69)$$

$$\vec{e} + N_2 \rightarrow 2N^{\bullet} \quad (70)$$

Toluene bond energy between the carbon of benzene ring and the carbon of the substituent radical is 3.6 eV, which is lower than that of carbon-carbon bond or hydrocarbon bond. As a hydrogen atom in a benzene ring is replaced by a methyl radical to form toluene, the newly formed bond is less stable and the most vulnerable. Of course, the other bonds are also likely to be destroyed by high energy electrons. Formulas 71 to 76 are the possible reaction equations of the process of toluene removal.


(71)

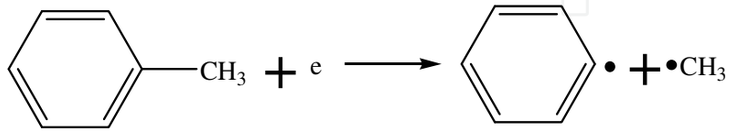
(72)

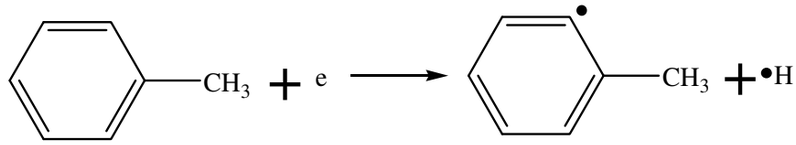
(73)

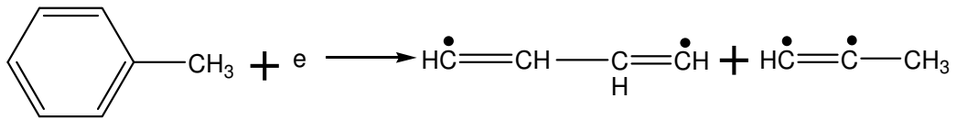
(74)

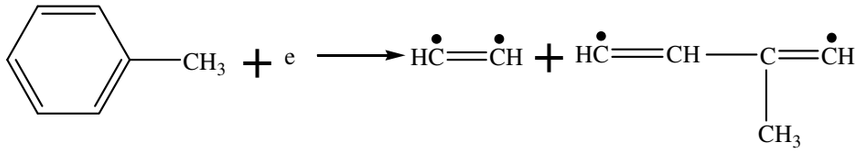
(75)


(76)

According to the FT-IR spectrums (Fig.40), the author speculated the reaction pathways for toluene decomposition with the NTP and the combination of catalysts (Fig.41). The oxygen and hydroxyl free radicals of should be the inducement during the process of toluene oxidation. The oxidation process of toluene may involve many reactions and these reactions cooperate and interact with each other for toluene decomposition. Firstly, a series of chain reactions take place between OH radicals and toluene molecules due to the higher oxidation ability of OH radicals than that of oxygen radicals:

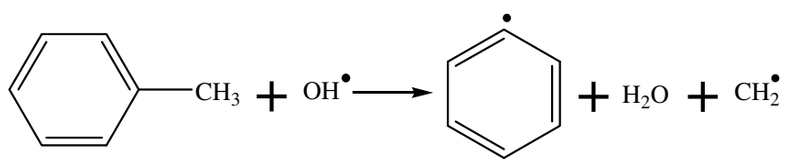
(77)

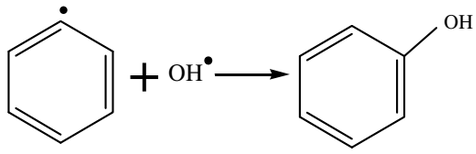
(78)

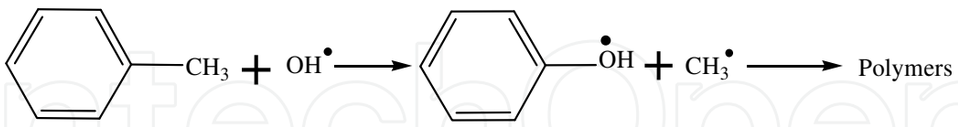
(79)

Then, the idiographic reactions occur because of oxygen free radicals during the subsequent oxidation reaction as follows:

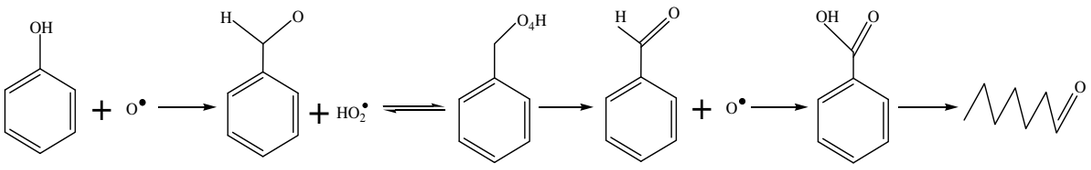
(80)

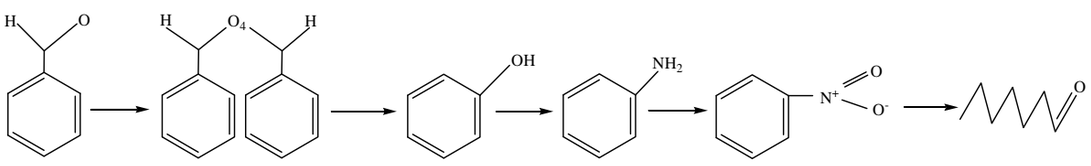
(81)

The binding bonds inside the benzene ring break down after the bonds outside the benzene ring break as follows:

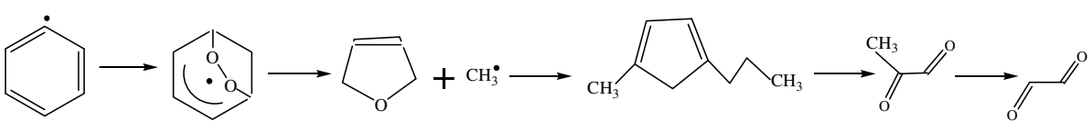
(82)

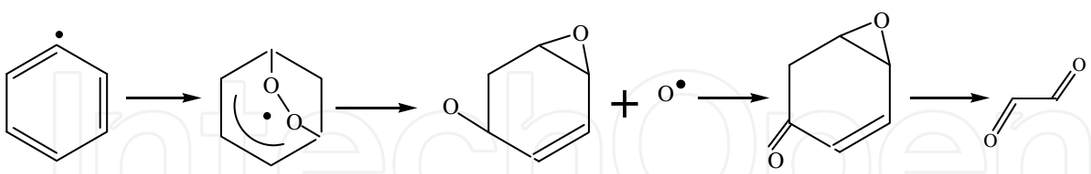
(83)

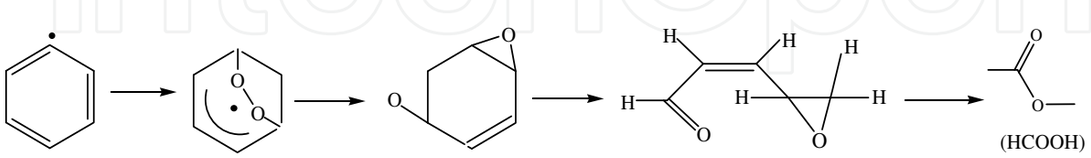
(84)

At last, the byproducts were oxidized to CO_2 and H_2O with increasing RED and the help of catalysis.

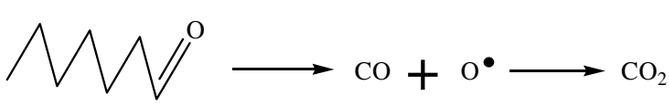
(85)

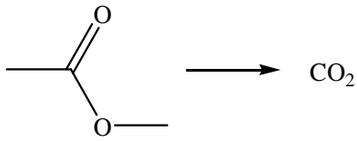

(86)

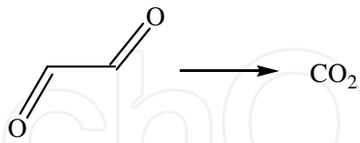

(87)

The byproducts of toluene decomposition were detected using GC-MS at electric field strength of 8 kV/cm and the results show the peak of these products in Fig.42 (a). Products including aldehyde, alcohols, amide, and benzene derivative have been identified.

Fig.42 (b) shows a minor amount of toluene and trace amounts of the products exist at electric field strength of 14 kV/cm. Chang et al. claimed that VOC removal depended on two main mechanisms: direct electrons attack on VOC molecules and indirect reaction between VOC molecules and radicals. These radicals involved oxygen plasma, free radical groups, ozone, etc., which were reactive and could react with toluene molecules to form less hazardous products. If the electric field strength was strong enough or RED was high enough, the toluene molecules would be oxidized to form CO_2, CO and H_2O as the final products.

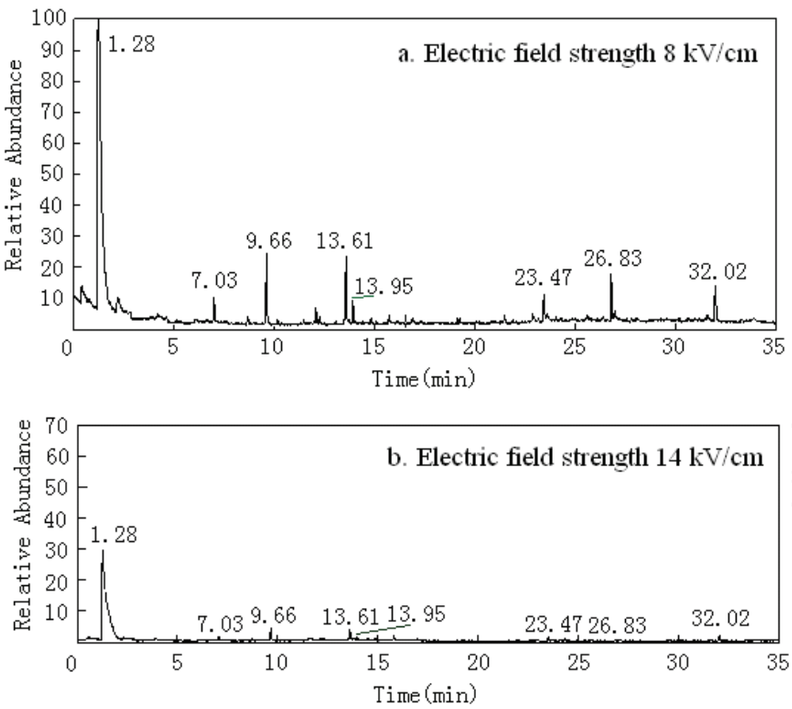

Fig. 42. Mass spectrum of byproducts of toluene decomposition

Atkinson *et al.* (1977) reported that aromatic compounds react with OH radicals by two pathways: hydrogen atom abstraction and OH addition to the aromatic ring. Reaction control pathways I–XII were illustrated in Fig.43. The results showed in a complex oxidation

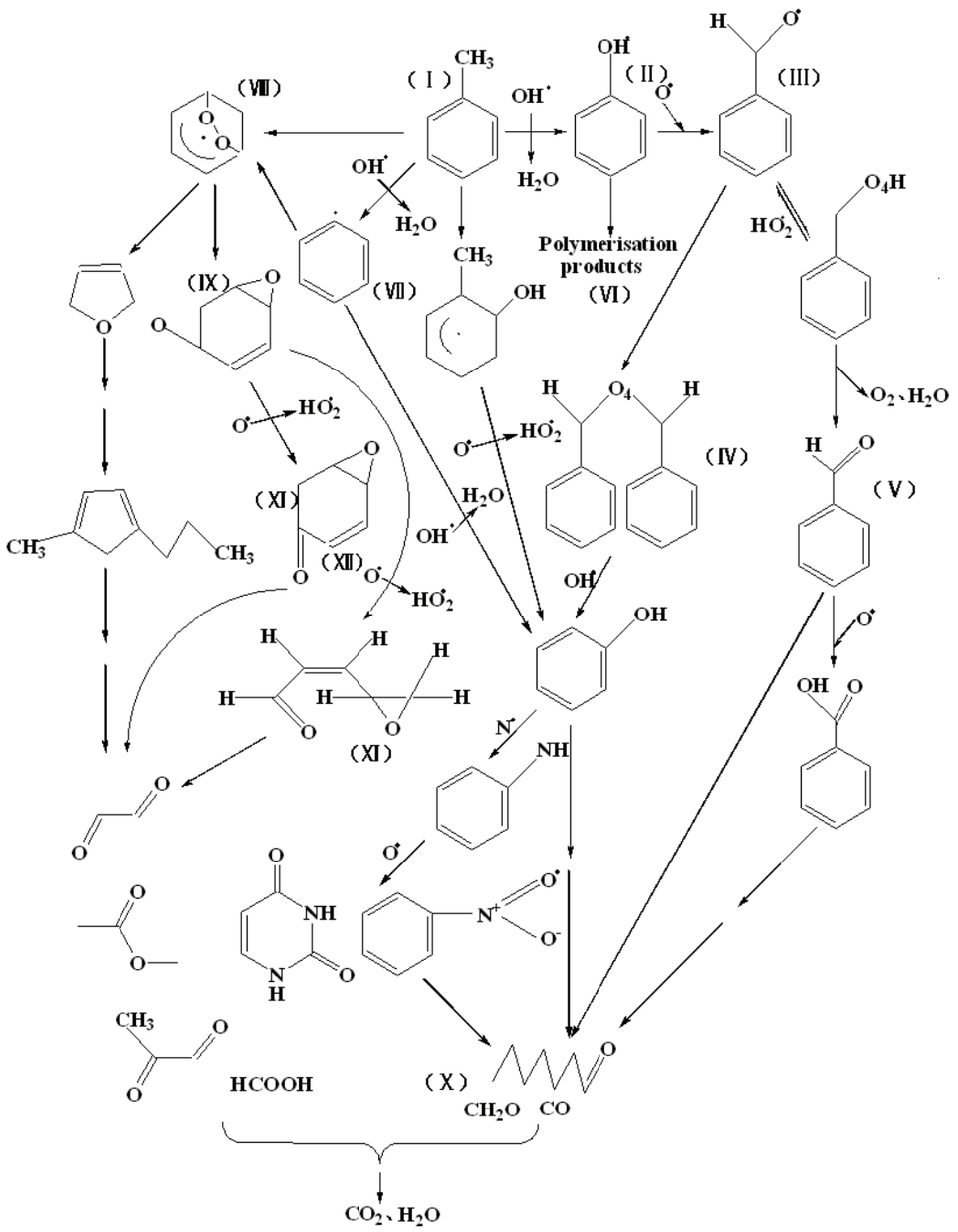

Fig. 43. Abatement pathways of toluene by NTP with the combination of catalysts

mechanism of toluene via several pathways, producing either ring-retaining or ring-opening products. The final products were CO_2 and H_2O.

The synergistic effect of the combination of catalysts with the NTP reactor is presented in Fig.44. The catalyst carrier of γ-Al_2O_3 possesses sorbent characteristic, so it could improve toluene concentration on the catalyst surface and increase the reaction time. MnO_2 is known as a metal oxide catalyst and has been reported to possess a potential activity in redox reactions. MnO_2 surface has been found to expose metal (Mn^{n+}), oxide (O^{2-}) and defect sites of various oxidation states, present degrees of coordination instauration, and exhibit acid and base properties. Furthermore, the d – d electrons exchange interactions between

intimately coupled manganese ions of different oxidation states [$Mn^{n+} - O - Mn^{(n+1)+}$] furnish the electron-mobile environment necessary for the surface redox activity:

$$O_3 + Mn^{n+} \rightarrow O_2^{2-} + Mn^{(n+2)+} + O_2 \quad (88)$$

$$O_3 + O^{2-} + Mn^{(n+2)+} \rightarrow O_2^{2-} + Mn^{(n+2)+} + O_2 \quad (89)$$

$$O_2^{2-} + Mn^{(n+2)+} \rightarrow Mn^{n+} + O_2 \quad (90)$$

These factors would be helpful for toluene decomposition. Radhakrishnan reported that ozone decomposed to O^{2-} and O_2^{2-} in the surface of MnO_2. Naydenov *et al*. believed that O^- existed in the surface of MnO_2 according to the oxidation of benzene in the surface of MnO_2. As a modified ferroelectric, nano-$Ba_{0.8}Sr_{0.2}Zr_{0.1}Ti_{0.9}O_3$ has a higher dielectric constant than $BaTiO_3$ and is polarized at lower electric field strength. More high energy electrons and active radicals are generated to accelerate the reaction between NTP and toluene molecules.

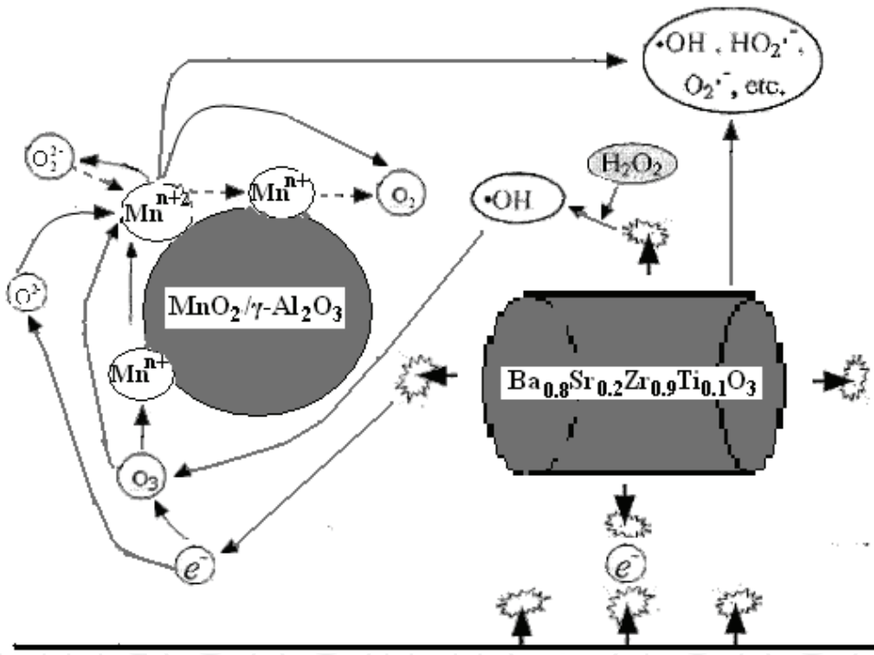

Fig. 44. Catalysis chart of the combination of catalysts in the process of gas discharge

7. Conclusions

In section secend, the adsorption kinetics was studied and the removal amount of VOCs was 25% or so through adsorption of γ-Al_2O_3. In the experiment, with the non-thermal plasma reactor size fixed, the immediate advantage of adsorption of the packed materials into the space of air discharge is the longer reaction time of VOCs with plasma and higher removal efficiency. The functions of γ-Al_2O_3 in plasma reactor were to adsorb free radicals and VOCs molecules and to provide reaction surface for VOCs decomposition and to release reaction products. Plasma decomposed air molecules and provided free radicals for catalysis

reactions on the surface of the γ-Al_2O_3 pellets. So adsorbent γ-Al_2O_3 enhanced NTP technology and resulted in higher VOCs removal efficiency and energy efficiency and a better inhibition for O_3 formation in the gas exhaust. For the study in the future, some catalysts should be considered to add into the NTP reactor.

In section third, a series of experiments for the effect of NTP technology were performed to abate toluene from a gaseous influent at room temperature and atmospheric pressure. Three types of NTP reactors were used in the NTP process for toluene removal with and without packed materials. A new modified ferroelectric material of $Ba_{0.8}Sr_{0.2}Zr_{0.1}Ti_{0.9}O_3$ as the packed materials was prepared by us in laboratory. Compared with the two packed materials in terms of removal efficiency of toluene, RED, energy efficiency and ozone concentration, the experimental results were obtained as follows: Packed materials with $Ba_{0.8}Sr_{0.2}Zr_{0.1}Ti_{0.9}O_3$ enhanced removal efficiency of toluene and energy efficiency than those with $BaTiO_3$. $Ba_{0.8}Sr_{0.2}Zr_{0.1}Ti_{0.9}O_3$ had better ferroelectric than $BaTiO_3$. By operating at the RED of 0.76 kJ/L, removal efficiency was up to 97% and the energy efficiency was 6.48 g/kWh when the packed materials of $Ba_{0.8}Sr_{0.2}Zr_{0.1}Ti_{0.9}O_3$ are used. O_3 concentration had a maximum value at the RED of 0.7 kJ/L or so. The hybrid NTP technology should be more effective to improve energy efficiency for VOCs removal than the simple technology of NTP. Based on the above results, we would consider how to control the formation of ozone in the further experiments. Our research would provide a reference to improve energy efficiency for the commercial applications of the NTP technology.

In section fourth, the laboratory-scale plasma reactor was used for benzene removal in an air stream and the following conclusions are obtained. B packed materials was better than A packed materials for benzene removal. Compared different size of packed materials, B packed materials of i.d.2 mm was better than the others' size for benzene decomposition.

In section fifth, nano-TiO_2 packed bed reactor is used to decompose benzene. The experimental results show as follows: With ozone concentration increasing, the removal efficiency of benzene increases. Ozone concentration with packed materials is heigher than that without packed materials in the plasma reactor. Water vapor reduces ozone concentration, and occurring competitive adsorption on the surface of TiO_2 Ozone concentration increases with gas flux increasing, and the removal efficiency of benzene reduces with initial concentration of benzene increasing. When both photocatalyst and ozone coexist, there will be an improved removal efficiency of benzene in the plasma reactor. Effective utilization of active oxygen species is essential in VOCs removal, and TiO_2 can generate higher concentrations of different types of active oxygen species in non-thermal plasma. It is facile and promising to simultaneously hybridize plasma with TiO_2 based on the data presented. The plasma reactor packed with catalyst (B packed materials coated nano-TiO_2) showed a better selectivity of CO_2. Detected by GC-MS, the main products in the plasma reactor are CO_2, H_2O and a small quantity of CO. The plasma reactor packed with catalyst shows a better selectivity of CO_2 than that without catalyst. The selectivity of CO_2 is independent of electrostatic field strength. The selectivity of CO_2 is enhanced due to the benzene oxidation near or on the photocatalyst surface. With benzene concentration increasing, the total output of CO_2 increases. The hybrid system comprising a non-thermal plasma reactor and nanometer TiO_2 catalyst, not only in the gas phase but on the catalyst surface, resulted in the higher energy efficiency and enhanced performance for the oxidative removal of benzene with lower medium reactivities and higher CO_2 selectivity in non-thermal plasma.

In section sixth, the synergistic effect of NTP and catalyst for VOCs removal is tested in the experiment. The results show that removal efficiency increased with increasing RED and was in the order of 10wt% MnO_2/γ-$Al_2O_3 \approx$ 15wt% MnO_2/γ-Al_2O_3 >5wt% MnO_2/γ-Al_2O_3 at the same RED. As the mass percentage of MnO_2 catalyst increased, ozone and VOCs concentrations were decreased, especially for 10 wt% MnO_2/γ-Al_2O_3. The removal efficiency and energy efficiency increased with increasing RED and was in the order of MnO_2/γ-Al_2O_3>TiO_2/γ-Al_2O_3>γ-Al_2O_3 at the same RED. So we could draw a conclusion that MnO_2/γ-Al_2O_3 has a better potential than the other catalysts in the experiment to improve the energy efficiency and reduce O_3 formation.
In section seventh, a series of experiments basing on above all researches, were performed for removal of toluene gaseous influent at room temperature and atmospheric pressure. The self-prepared combined catalyst was used to improve the NTP process and to take the catalytic advantages of both MnO_2/γ-Al_2O_3 and nano-$Ba_{0.8}Sr_{0.2}Zr_{0.1}Ti_{0.9}O_3$. From the view of materials application, the authors adopted NTP coupled with the combination of catalysts technology to decompose VOCs in there. The catalyst materials could be prepared easily and cheap, and at the same time, this combined technology resolved the key bottlenecks effectively, i.e. saving energy consumption and reducing byproducts what we don't want. Therefore, the combination of catalysts technology could advance to the NTP technology and improve applications in the industry in the future.

8. Acknowledgements

This work was supported by the Youth Research Funding of China University of Mining & Technology (Beijing), and China College of innovative pilot projects (No.101141309), and the Fundamental Research Funds for the Central Universities (No.2009QH03), and Environmental Protection Commonweal Industry Research Special Projects (No.201009052-02), and the Doctoral Program of Higher Education of China (20040005009).

9. References

Atkinson R., Pitts J.N. (1977). Jr. "Kinetics and mechanism of the gas phase reaction of hydroxyl radicals with aromatic hydrocarbons over the temperature range 296-473 K". *J. Phys. Chem.* 81, 296–304.

Ayrault C., Barrault J., Blin-Simiand N., Jorand F., Pasquiers S., Rousseau A., Tatibouet J.M. (2003): Oxidation of 2-heptanone in air by a DBD type plasma generated within a honeycomb monolith supported Pt-based catalyst, Cata. Today. 89: 75-83.

Chang M.B., Balbach J.H., Rood M.J., Kushner M.J. (1991). "Removal of SO_2 from gas streams using a dielectric barrier discharge and combined plasma photolysis". *J. Appl. Phys.*, 69, 4409-4418.

Chang M.B., Lee C.C. (1995): Destruction of formaldehyde with dielectric barrier discharge plasmas, Environ. Sci. Tech. 29: 181-186.

Chang M.B., Tseng T.D. (1996). "Gas-phase removal of H_2S and NH_3 with dielectric barrier discharges". *J. Environ. Eng.*, 122, 41-46.

Delagrange S., Pinard L., Tatiboue¨t J.M. (2007): Combination of a non-thermal plasma and a catalyst for toluene removal from air: Manganese based oxide catalysts, Appl. Catal. B: Environ. 68: 92-98.

Ding S.W., Wang J., Qin J.L. (2001). "The structure and performance of complex of nanometer $BaTiO_3$". Sci. China, Ser. B. 31, 525-529.

Eliasson B., Kogelschatz U. (1991): Nonequilibrium volume plasma chemical processing, IEEE Trans. Plasma Sci. 19: 1063-1068.

Einaga H., Lbusuki T., Futamura S., 2001. Performance evaluation of a hybrid system comprising silent discharge plasma and manganese oxide catalysts for benzene decomposition. *IEEE Tran. Ind. Appli.* 37 (5), 858-863.

Futamura S., Zhang A.H., Yamamoto T. (1997). "The dependence of nonthermal plasma behavior of VOCs on their chemical structures". *J. Electrostat.*, 42, 51-62.

Futamura S., Einaga H., Kabashima H. (2004). "Synergistic effect of silent discharge plasma and catalysts on benzene decomposition". *Catal. Today*, 89, 89-95.

Gal A., Ogata A., Futamura S. (2003). "Mechanism of the dissociation of chlorofluorocarbons during nonthermal plasma processing in nitrogen at atmospheric pressure". *J. Phys. Chem. A*, 107, 8859-8866.

Guo Y.F., Ye D.Q., Chen K.F. (2006). "Toluene decomposition using a wire-plate dielectric barrier discharge reactor with manganese oxide catalyst in situ". *J. Molecular Cata. A: Chem.* 245, 93-100.

Guo Y.F., Ye D.Q., Chen K.F., He J.C. (2007). Toluene removal by a DBD-type plasma combined with metal oxides catalysts supported by nickel foam. Catal. Today, 126(3-4), 328~337.

Kim H.H. (2006). "Effect of different datalysts on the decomposition of VOCs using flow-type plasma-driven catalysis". *IEEE Trans. Plasma Sci.*, 34, 984-995.

Kim H.H., Ogata A., Futamura S. (2008). "Oxygen partial pressure-dependent behavior of various catalysts for the total oxidation of VOCs using cycled system of adsorption and oxygen plasma". *Appl. Catal. B: Environ*. 79, 356-367.

Kohno H., Berezin A.A., Chang J.S. (1998). "Destruction of volatile organic compounds used in a semiconductor industry by a capillary tube discharge reactor". *IEEE Trans. Ind. Appl.* 34 953-966.

Krawczyk K., Mlotek M. (2001). Combined plasma-catalytic processing of nitrous oxide. Appl. Catal. B: Environ., 30(3-4), 233-245.

Li C.Y., Li M.Q. (1996). Study on Sol-Gel transition of TiO_2. J. Chinese Ceramic Society, 24(3), 338-341.

Li G.W., Fan Q.J., Liu Q. (1998). The control technique over the pollution caused by VOCs. J. Xi'an Univ. of Arch & Tech. 30(4), 399-402.

Li J., Ma G.D., 2000. The mechanismic analysis and experiment on controlling volatile organic compounds (VOCs) with corona discharge. *J. Xi'an Univ. of Arch & Tech.*, 32 (1), 24-27.

Li R., Tang Q., Yin S., Sato T. (2006). Plasma catalysis for CO_2 decomposition by using different dielectric materials. Fuel Proc. Tech., 87(7), 617–622.

Li W., Han C., Liu W., Zhang M.H., Tao K.Y. (2007). Expanded graphite applied in the catalytic process as a catalyst support. Catal. Today, 125(3-4), 278-281.

Liang Y.H., Zhu T., Ma G.D., 2006. Study of nano-TiO_2 thin film derived by sol-gel process. *J. Xi'an Univ. of Arch. & Tech.*, 38 (6), 799-803.

Ma G.D. (2003). Air Pollution Control Engineering (second edition). Beijing, China Environ. Sci. Press. 105-134.

Magureanu M., Mandache N.B., Hu J.C., Richards R., Florea M., Parvulescu V.I. (2005): Plasma-assisted catalysis for volatile organic compounds abatement, Appli. Cata. B: Environ. 61: 12-20.

Magureanu M., Mandache N.B., Subrahmanyam C., Kiwi-Minsker L. (2007): Improved performance of non-thermal plasma reactor during decomposition of trichloroethylene: Optimization of the reactor geometry and introduction of catalytic electrode, Appl. Catal. B: Environ. 74: 270-283.

Magureanu M., Mandache N. B., Hu J.C., Richards R., Florea M., Parvulescu V.I. (2007). Plasma-assisted catalysis total oxidation of trichloroethylene over gold nano-particles embedded in SBA-15 catalysts. Appl. Catal. B: Environ.,76(3-4), 275-281.

Malik M. A., Minamitani Y., Schoenbach K. H. (2005). "Comparison of catalytic activity of aluminum oxide and silica gel for decomposition of volatile organic compounds (VOCs) in a plasmacatalytic reactor". *IEEE Trans. Plasma Sci*., 33 (1), 50-56.

Masuda S., 1988. Pulse corona induced plasma chemical process: a horizon of new plasma chemical technologies. *Pure Appl. Chem.*, 60 (5), 727-731.

Masuda S., Hosokawa S., Tu X.L., Tsutsumi M., Ohtani T., Tsukahara T., Matsuda N., 1993. The performance of an integrated air purifier for control of aerosol, microbial, and odor. *IEEE Trans. Ind. Appl*., 29 (4), 774-780.

Maria D., Hernandez A., Juan M.C., Maira A.J., Soria J., Loddo V., Augugliaro V. (2002). Ozone enhanced activity of aqueous titanium dioxide suspensions for photocatalytic oxidation of free cyanide ions. Appl. Catal. B: Environ., 39(3), 257-267.

Mizuno A., Clements J.S., Davis R.H., 1986. A method for the removal of sulfur dioxide from exhaust gas utilizing pulsed streamer corona for electron energization. *IEEE Trans. Ind. Appl*., 22 (3), 516-522.

Mizuno A., Yamazaki Y., Obama S., 1993. Effect of voltage waveform on partial discharge in ferroelectric pellet layer for gas cleaning. *IEEE Trans. Ind. Appl*., 29 (2), 262-267.

Muhamad A.M., Jiang X.Z., 2000. Catalyst assisted destruction of trichloro ethylene and toluene in corona discharges. *J. Environ. Sci*., 12 (1), 7-11.

Naydenov A., Mehandjiev D.. (1993). "Complete oxidation of benzene on manganese dioxide by ozone". App1.Cata1.A: Gen, 97, 17-22.

Noel D.N. (2000). Air Pollution Control Engineering (second edition). Beijing, McGraw-Hill. 329-382.

Nunez C M, Ramsey G H, Ponder W H, Abbott J H, Hamel L E, Kariher P H. (1993). "Corona destruction: An innovative control technology for VOCs and air toxics". Air & Waste, 43 (2), 242-247.

Ogata A., Yamanonchi K., Mizuno K. (1999). "Decomposition of benzene using alumina-hybrid and catalyst-hybrid plasma reactors". *IEEE Tran. Ind. Appli.* 35, 1289-1295.

Ogata A., Einaga H., Kabashima H. (2003). "Effective combination of nonthermal plasma and catalysts for decomposition of benzene in air". *Appl. Catal. B: Environ.* 46, 87-95.

Ohkubo T., Kanazawa S., Nomoto Y., 1994. NOx removal by a pipe with nozzle-plate electrode corona discharge system. *IEEE Trans. Ind. Appl*., 30 (4), 856-861.

Park J.Y., Jung J.G., Kim J.S. (2003). "Effect of nonthermal plasma reactor for CF decomposition". *IEEE Trans. Plasma Sci*., 31, 1349-1354.

Rachel F. (1998): Automated system for power measurement in the silent discharge, IEEE Trans. Ind. Appl. 34: 563-570.

Radhakrishnan R., Oyama S.T., Chen J.G. (2001). "Electron transfer effects in ozone decomposition on supported manganese oxide". J.Phys.Chem.B, 105, 4245-4253.

Ricketts C.L., Wallis A.E., Whitehead J.C. (2004): A mechanism for the destruction of CFC-12 in a nonthermal, atmospheric pressure plasma, J. Phys. Chem. A. 108: 8341-8345.

Subrahmanyam Ch., Renken A., Kiwi-Minsker L. (2007). "Novel catalytic non-thermal plasma reactor for the abatement of VOCs". Chem. Eng. J. 134, 78-83.

Thevenet F., Guaitella O., Puzenat E., Herrmann J.M., Rousseau A., Guillard C. (2007). Oxidation of acetylene by photocatalysis coupled with dielectric barrier discharge. Catal. Today, 122(1-2), 186-194.

Tonkyn R.G., Barlow S.E., Orlando T.M. (1996). "Destruction of carbon tetrachloride in a dielectric barrier/packed-bed corona reactor". *J. Appl. Phys.*, 80, 4877-4886.

Tonkyn R.G., Barlow S.E., Hoard J. (2003). "Reduction of NOx in synthetic diesel exhaust via two-step plasma-catalytic treatment". *Appl. Catal. B: Environ.*, 40, 207-217.

Urashima K., Chang J. (2000). "Removal of volatile organic compounds from air streams and industrial flue gases by non-thermal plasma technology". *IEEE Trans. Dielectr. Electr. Insul.*, 7, 602-614.

Van Durmea J., Dewulfa J., Sysmansa W., Leysb C., Van Langenhove H. (2007). „Efficient toluene abatement in indoor air by a plasma catalytic hybrid system". *Appl. Cata. B: Environ*. 74, 161-166.

Van Durme J., Dewulf J., Leys C., Langenhove H. (2008): Combining non-thermal plasma with heterogeneous catalysis in waste gas treatment: A review, Appl. Cata. B: Environ. 78: 324-333.

Wallis A.E., Whitehead J.C., Zhang K. (2007). The removal of dichloromethane from atmospheric pressure air streams using plasma-assisted catalysis. Appl. Catal. B: Environ., 72(3-4), 282-288.

Yamamoto T., Ramanatiran K, Lawless P. A., Ensor D.S., Nwesome J. R., Plaks N., Ramsey G. H. (1992). "Control of Volatile organic compound by ac energized ferroelectric pellet reactor and a pulsed corona reactor". *IEEE Trans Ind Appl*, 28(3), 528-533.

Yamamoto T., Mizuno K., Tamori I., Ogata A., Nifuku M., Michalska M., Prieto G., (1996). "Catalysis-assisted plasma technology for carbon tetrachloride destruction". *IEEE Trans Ind Appl*, 32(1), 100-106.

Yamamoto T. (1997): Methods and apparatus for controlling toxic compounds using catalysis-assisted non-thermal plasma, Environ. Int. 23: 3-10.

Yoichi I., Junya S., Takashi N., Shigeyoshi M. (2008). Synthesis of visible-light active TiO_2 photocatalyst with Pt-modification: Role of TiO_2 substrate for high photocatalytic activity. Appl. Catal. B: Environ., 79(2), 117-121.

Young S.M., Mirosław D., Jerzy M. (2004). "Effect of reaction temperature on NOx removal and formation of ammonium nitrate in nonthermal plasma process combined with selective catalytic reduction". *IEEE Trans. Plasma Sci.*, 32, 799-807.

Zhu T., Li J., Dou B.J., Liang W.J., Jin Y.Q., 2007. Study on treatment tobacco odor with non-thermal plasma technology. *J. Xi'an Univ. of Arch. & Tech.*, 39 (6), 862-866.

Zhu T., Li J., Liang W.J., Dou B.J., Jin Y.Q. (2007). Gaseous phase toluene decomposition by non-thermal plasma. Environ. Pollution & Protection, 29(12), 920-924.

Zhu T., Li J., Dou B.J., Liang W.J., Jin Y.Q. (2007). Study on treatment tobacco odor with non-thermal plasma technology. J. Xi'an Univ. of Arch & Tech., 39(6), 862-866.

Zhu T., Li J., Liang W.J., Jin Y.Q. (2008). Research Progresses in treatment of waste gas containing volatile organic compounds by combined plasma technology. Environ. Protec. Chem. Ind., 28(2): 121-125.

Zhu T., Li J., Liang W.J., Dou B.J., Jin Y.Q., 2008. Research Progresses in Treatment of Waste Gas Containing Volatile Organic Compounds by Combined Plasma Technology. *Environ. Protec. Chem. Ind.* 28 (2), 121-125.

Zhu T., Li J., Jin Y.Q., Liang Y.H., Ma G.D. (2008). "Decomposition of benzene by non-thermal plasma processing-photocatalyst and ozone effect". *Int. J. Environ. Sci. Tech.* 5, 375-384.

Zhang D.Y., Pan X.L., Li L.H., Song W.J., Wu G.Y., Liu J. (2010) Glow plasma degradation of aqueous direct black 38, Fresenius Environ. Bulletin.19: 1-7.

Zhu T., Li J., Jin Y.Q., Liang Y.H., Ma G.D. (2009). „Gaseous phase benzene decomposition by nonthermal plasma coupled with nano-titania catalyst". *Int. J. Environ. Sci. Tech.* 6, 141-152.

Zhu T., Li J., Liang W.J., Jin Y.Q. (2009). "Synergistic effect of catalyst for oxidation removal of toluene". *J. Hazardous Materials*. 165, 1258-1261.

Zhu T., Xu D.Y., He X.W., Shu X.Q. (2010): Decomposition of benzene in dry air bu super-imposed barrier discharge nonthermal plasma-photocatalytic system, Fresenius Environ. Bulletin. 19: 1275-1282.

Zhu T., Wan Y.D., He X.W., Xu D.Y., Shu X.Q. (2011). "Effect of modified ferroelectric on nonthermal plasma process for toluene decomposition". *Fresenius Environmental Bulletin*. 20(1), 149-155.

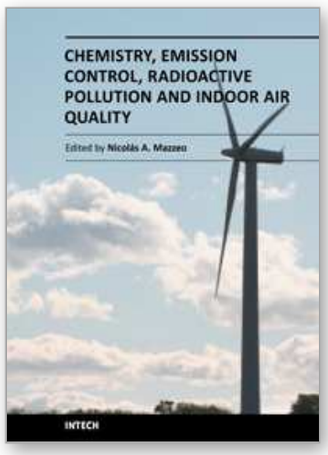

Chemistry, Emission Control, Radioactive Pollution and Indoor Air Quality

Edited by Dr. Nicolas Mazzeo

ISBN 978-953-307-316-3
Hard cover, 680 pages
Publisher InTech
Published online 27, July, 2011
Published in print edition July, 2011

The atmosphere may be our most precious resource. Accordingly, the balance between its use and protection is a high priority for our civilization. While many of us would consider air pollution to be an issue that the modern world has resolved to a greater extent, it still appears to have considerable influence on the global environment. In many countries with ambitious economic growth targets the acceptable levels of air pollution have been transgressed. Serious respiratory disease related problems have been identified with both indoor and outdoor pollution throughout the world. The 25 chapters of this book deal with several air pollution issues grouped into the following sections: a) air pollution chemistry; b) air pollutant emission control; c) radioactive pollution and d) indoor air quality.

INTECH
open science | open minds

InTech Europe
University Campus STeP Ri
Slavka Krautzeka 83/A
51000 Rijeka, Croatia
Phone: +385 (51) 770 447
Fax: +385 (51) 686 166
www.intechopen.com

InTech China
Unit 405, Office Block, Hotel Equatorial Shanghai
No.65, Yan An Road (West), Shanghai, 200040, China
中国上海市延安西路65号上海国际贵都大饭店办公楼405单元
Phone: +86-21-62489820
Fax: +86-21-62489821

IntechOpen